NASA TECHNICAL NOTE

NASA TN D-2302

HEAT-TRANSFER DISTRIBUTION ON 70° SWEPT SLAB DELTA WINGS AT A MACH NUMBER OF 9.86 AND ANGLES OF ATTACK UP TO 90°

by Philip E. Everhart and James C. Dunavant

Langley Research Center
Langley Station, Hampton, Va.

HEAT-TRANSFER DISTRIBUTION ON 70° SWEPT SLAB DELTA WINGS

AT A MACH NUMBER OF 9.86 AND ANGLES OF ATTACK UP TO 90°

By Philip E. Everhart and James C. Dunavant

Langley Research Center
Langley Station, Hampton, Va.

HEAT-TRANSFER DISTRIBUTION ON 70° SWEPT SLAB DELTA WINGS

AT A MACH NUMBER OF 9.86 AND ANGLES OF ATTACK UP TO 90°

By Philip E. Everhart and James C. Dunavant
Langley Research Center

SUMMARY

Heat-transfer distributions were obtained on 70° swept slab delta wings with sharp and blunt noses and cylindrical leading edges. The free-stream Reynolds number based on model thickness was 9×10^4. Lees' theory for the heat-transfer distribution is shown to be in good agreement with the data obtained on the nose and leading edge. The point of peak heating on the leading edge is in close agreement with the Newtonian stagnation point at all angles of attack. At angles of attack from 40° to 60° cross-flow theory was in excellent agreement with experimental center-line data; however, at other model attitudes the theory differed significantly from experiment. Nose blunting resulted in reduced heating rates over the aft center-line section of the wing at angles of attack less than about 40°.

INTRODUCTION

A systematic research program was initiated at the Langley Research Center to provide detailed heat-transfer and pressure distributions for delta wings over a wide range of Mach numbers and angles of attack. Low angle-of-attack heat-transfer and pressure distributions obtained under this program are presented in references 1 to 3. Pressure distributions have been measured at high angles of attack (up to 90° and beyond) on blunt leading-edge delta wings and are presented in references 4 to 6. Heat-transfer tests on sharp delta wings at angles of attack approaching 90° are reported in references 7 and 8. Heat-transfer and pressure distributions on 70° delta wing configurations at a Mach number of 20 and angles of attack from 0° to 90° are presented in reference 9.

The purpose of the present investigation was to provide detailed heat-transfer distributions at high angles of attack on 70° swept slab delta wings with cylindrical leading edges and both sharp and blunt noses. This investigation was carried out in the Langley continuous-flow hypersonic tunnel at a Mach number of 9.86, a Reynolds number based on model thickness of 0.9×10^5, and for angles of attack from 0° to 90°.

Heat-transfer data were obtained by means of a transient calorimeter method and a model-injection mechanism. The heat-transfer data are compared with the

theories for swept cylinders, spheres, and flat plates. Lees' theory is compared with the results in the nose and leading-edge regions whereas the results on the slab are compared with cross-flow and strip theories.

SYMBOLS

a	speed of sound
C_p	Newtonian pressure coefficient
c_w	specific heat of model skin material
C_w	coefficient in linear expansion for viscosity (Fay and Riddell)
h	aerodynamic heat-transfer coefficient
j	index number
L	distance along leading edge measured from apex of slab portion of wing
M	Mach number
N_{St}	Stanton number
N_{Pr}	Prandtl number
p	static pressure
q	heat-transfer rate
$R_{\infty,t}$	Reynolds number based on model thickness and free-stream conditions
s	surface distance along wing normal to leading edge from Newtonian stagnation point
s_c	surface distance along wing center line from Newtonian stagnation point
s_n	surface distance along wing normal to leading edge measured from plane of symmetry of leading edge
s_0	total surface distance along wing normal to leading edge from midline of wing to center line of wing
t_w	model skin thickness
t	model slab thickness, diameter of nose and leading edge

T	temperature
T_{aw}	adiabatic wall temperature
u	velocity
α	angle of attack
γ	ratio of specific heats of air taken to be 1.4
η_r	temperature recovery factor
ρ	density
τ	time
μ	viscosity
Λ	sweep angle
Λ_{eff}	effective sweep angle, $\sin \Lambda_{eff} = \sin \Lambda \cos \alpha$

Subscripts:

2	static conditions just behind normal shock
cf	cross flow
l	local static conditions just outside boundary layer
max	maximum
N	normal to leading edge
O	stagnation-point values
s	sphere
w	wall material
∞	free-stream conditions

APPARATUS AND TESTS

Tunnel

The heat-transfer tests were conducted in the Langley continuous-flow hypersonic tunnel. Photographs of this facility are shown in figure 1. This

facility is capable of maintaining a Mach number of 10 continuously by circulating the air through a closed loop of compressors. In normal operation the high-pressure ratio required to start the nozzle is supplied by a high-pressure air storage system on one end and a vacuum tank downstream. The flow is diverted to the compressor loop within 30 seconds after the flow is initiated and the movable second minimum is closed and thus the pressure ratio required to maintain flow is reduced. Since the time required for the heat-transfer tests was only a few seconds (for model injection), the facility was operated by using the high-pressure stored air and the vacuum sphere.

In the present tests a contoured three-dimensional, water-cooled nozzle with a square throat and a 31-inch-square test section was used. The nozzle had a calibrated Mach number of 9.86 ± 0.10 over a 12-inch by 12-inch core at a stagnation chamber pressure of 600 pounds per square inch. The test-section Mach number was obtained from total-pressure measurements.

Models

Four delta-planform slab-wing models were constructed with 70° sweep and cylindrical leading edges. Two of the models had sharp noses formed by the intersection of the elements of the cylindrical leading edge on the wing center line. The other two models had blunt noses and the apex was formed by a sphere tangent to the two leading edges and having the same diameter as the cylindrical leading edge. The general configuration of the models is shown by the photograph (fig. 2(a)) and pertinent dimensions are given in the detailed drawings (figs. 2(b) and 2(c)). The larger models (models 1 and 2) shown in figure 2(b) were tested through an angle-of-attack range of 0° to 30° whereas the smaller models (models 3 and 4 in fig. 2(c)) were tested at angles of attack from 30° to 90°.

The models were constructed from inconel in sections and then welded together. The leading edges were machined with a cylindrical outer surface and eccentric cylindrical inner surface so that the skin thickness varied along the circumference of the cylinder; the skin thickness over the spherical nose of the blunt models was similarly varied. (See fig. 3.) The slab surfaces were formed from sheet inconel. Models 1 and 2 had nominal skin thicknesses of 0.040 inch on the windward side and 0.025 inch on the leeward side. Models 3 and 4 had nominal slab skin thicknesses of 0.050 inch on the windward side and 0.025 inch on the leeward side. The variation of skin thickness around the models was designed to reduce the variation in temperature around the model. The wings were assembled by electron beam welding the leading edges to the slabs. The two large models were sting mounted from the model base; the two smaller models were attached to offset adapters on the leeward side of the model at angles of 30° and 75° to the plane of the wing.

The location of the individual thermocouples is shown in figures 2(b) and 2(c). The thermocouples were 0.010-inch-diameter chromel-alumel wire fastened to the model nose and leading edges by welding a preformed bead into a hole drilled through the skin. The slab regions were instrumented by spotwelding individual wires to the inside of the skin. The instrumentation is laid out

normal to the leading edge and on the slab the thermocouples are also arranged on rays from the slab apex.

Tests

Heat-transfer data were obtained at a free-stream Mach number of 9.86 for angles of attack from 0° to 90°. Models 1 and 2 were tested at a stagnation pressure of 600 pounds per square inch which gave a Reynolds number based on model thickness (1.0 inch) of about 0.9×10^5 for angles of attack from 0° to 30°. For angles of attack from 30° to 90°, models 3 and 4 were tested at a stagnation pressure of 800 pounds per square inch (Reynolds number based on model thickness (0.73 inch) of about 0.9×10^5). The stagnation temperature was maintained at an average value of 1175° F by means of an electrical resistance-tube heater. Details of the test conditions are given in table I.

TABLE I.- TEST CONDITIONS

$$\left[M_\infty = 9.86\right]$$

Run	Chord length, in.	α, deg	T_0, °R	p_0, lb/sq in. abs	$R_{\infty,t}$
Sharp-nose configuration					
3	11	0	1670	609	0.90×10^5
6	11	10	1682	607	.88
7	11	20	1601	610	.97
9	11	30	1648	600	.95
15	8	90	1642	742	.80
16	8	80	1582	754	.86
17	8	70	1614	780	.86
18	8	60	1629	791	.87
19	8	50	1553	812	.98
20	8	40	1539	808	1.00
21	8	30	1577	807	.93
Blunt-nose configuration					
22	11	0	1609	607	1.10×10^5
23	11	10	1714	606	.84
26	11	20	1638	593	.90
27	11	30	1629	589	.90
28	8	90	1552	806	.97
29	8	80	1578	806	.91
30	8	70	1566	806	.93
31	8	60	1583	802	.91
32	8	50	1522	804	1.00
33	8	40	1632	796	.86
34	8	30	1649	794	.84

The heat transfer was measured by means of a transient heating method using a model-injection mechanism which was mounted on the side of the test section at one of the window openings. The tunnel was started and brought to the desired operating conditions with the model outside the test section. A vertical door, which covered the test-section opening, was retracted and the model, oriented at the desired angle of attack, was injected into the tunnel. The time from the moment the model was first exposed to the flow until it reached the center line of the test section was approximately 1/4 second. Data recording began simultaneously with the start of model insertion and continued for 6 seconds after the model reached the center line of the tunnel. The temperature-time data and tunnel flow conditions were automatically recorded on magnetic tape by an analog-to-digital converter at 0.05-second intervals. After the temperature-time history was recorded, the model was retracted and cooled to approximately room temperature before the succeeding run.

Data Reduction

The data reduction was performed on an automatic card program machine. Temperature-time curves were plotted for selected thermocouples to determine the time at which the initial transient temperature rise was completed. The heat-transfer rate at 0.5 second* after this completion was determined by fitting a quadratic least-squares curve to 21 consecutive points centered about this time and spaced at intervals of 0.05 second. The temperature-time derivative obtained by differentiating the equation was used in the following equation to determine the heat-transfer rate:

$$q = \rho_w c_w t_w \frac{dT_w}{d\tau} = h\left(T_{aw} - T_w\right) \qquad (1)$$

Values of the effective skin thickness were calculated from skin thicknesses measured during fabrication and the appropriate spherical or cylindrical radius for use in equation (1). The value of specific heat corresponding to the model temperature was used in equation (1). The values of specific heat were obtained from the following empirical equation:

$$c_w = 0.1041 + 0.000033T_w, \text{ Btu/lb-}^\circ F$$

where T_w is in degrees Fahrenheit. The skin-density value was 0.307 lb/in.[3]

Adiabatic wall temperatures T_{aw} were estimated for each thermocouple location from the relation:

---

*The initial transient temperature rise on the hemispherical nose of model 2 was longer than at other stations because of the very thick wall. To avoid these transients, the heating was calculated 1 second later at these few locations.

$$\frac{T_{aw}}{T_0} = \frac{1 + \eta_r \frac{\gamma - 1}{2} M_l^2}{1 + \frac{\gamma - 1}{2} M_l^2}$$

The recovery factor was calculated from the square root of the Prandtl number which was estimated to be 0.70. Local Mach numbers were determined from the measured pressures of reference 1 for angles of attack from 0° to 30° and Newtonian $\left(C_{p,max} = 2.0\right)$ pressure distributions were used for angles of attack from 40° to 90°. The entropy rise across the appropriate shock was taken into account. For the sphere a normal shock was used and for the cylindrical leading edge and slab a swept-cylinder entropy rise was assumed.

Estimates of the lateral conduction of several thermocouple stations where conduction was expected to be a maximum were calculated by the method in reference 1. The results indicated that the conduction correction to the data would be less than 5 percent of the measured rates; the data are therefore presented uncorrected.

RESULTS AND DISCUSSION

Spherical Nose

Heat-transfer rates along the center line of the blunt (spherical nose) models are presented in figure 4 in terms of the parameter $N_{St,\infty}\sqrt{R_{\infty,t}}$ based on free-stream conditions as in the earlier tests of this series. The distance parameter s_c/t is the surface distance along the wing center line from the Newtonian stagnation point in terms of model thickness. The flagged symbols indicate the attitude at which tests for the high angle-of-attack model (model 4) overlap those for the low angle-of-attack model (model 2). The data for the two models at this angle of attack generally compare favorably; however, in some instances, as shown in figure 4 at $s_c/t = 0.524$, considerable difference exists between the heating measured on the two models. The point of maximum heating, in general, follows the movement of the Newtonian stagnation point ($s_c/t = 0$) as angle of attack is varied and the overall heating distribution is consistent with that predicted by Lees' theory for the isolated sphere. The maximum rate of heating is shown to vary by a factor of 2 over the range of these tests; at the two high angles of attack ($\alpha = 80^\circ$ and 90°) the maximum rate drops rapidly as the flow stagnation point moves toward the slab surface.

Cylindrical Leading Edge

The variation of maximum heat-transfer parameter with angle of attack is shown in figure 5. These maximum values were obtained close to the Newtonian

stagnation line of the component of the flow normal to the leading edge, here-inafter called Newtonian stagnation line. In general, the measured heating along the leading edge of both the sharp- (fig. 5(a)) and blunt-nose (fig. 5(b)) models increased with angle of attack up to about 40° and leveled off at the higher angles of attack.

The data at the $L/t = 0$ station are higher than the other leading-edge data, particularly at the high angles of attack. The compactness of the leading-edge data, for L/t stations from 1 to 9 on the sharp-nose models (fig. 5(a)), indicates a slight change in heating along the leading edge at angles of attack less than about 30°. The decrease of the heating along the leading edge of the sharp-nose model at higher angles of attack is shown by the spread of the data; however, the data at the most rearward stations ($L/t = 6$ to 9) show little change in the heating.

The data are compared with theoretical values obtained from adaptations of the theories of Fay and Riddell and Sibulkin for heat transfer at the stagnation point of a blunt body. These values were obtained from the equations of reference 1 by using a value of the geometric stagnation-point velocity gradient,

$$\left[\frac{d(u/a_0)}{d(s/t)}\right]_0$$ equal to 2.18. From the theory of Fay and Riddell,

$$\left(N_{St,\infty}\sqrt{R_{\infty,t}}\right)_0 = \frac{0.54(2)^{j/2}}{N_{Pr}^{0.6}}\, C_w^{0.1}\sqrt{\frac{p_0}{p_\infty}\frac{\mu_0}{\mu_\infty}\left(\frac{T_\infty}{T_0}\right)^{1/2}\frac{1}{M_\infty}\left[\frac{d(u/a_0)}{d(s/t)}\right]_0} \qquad (2)$$

in which $j = 0$ for a cylinder and $j = 1$ for a sphere and where $C_w = \dfrac{\mu_w T_0}{\mu_0 T_w}$.

From the theory of Sibulkin,

$$\left(N_{St,\infty}\sqrt{R_{\infty,t}}\right)_0 = \frac{0.763(0.747)^{1-j}}{N_{Pr_2}^{0.6}}\sqrt{\frac{\mu_2}{\mu_\infty}\frac{a_0}{u_2}\left(\cos \Lambda_{eff}\right)^{1-j}\left[\frac{d(u/a_0)}{d(s/t)}\right]_0} \qquad (3)$$

Although both the Fay and Riddell and the Sibulkin theories for cylinders under-estimate the maximum heat transfer on both the sharp- and blunt-nose models at angles of attack from 0° to 20° (figs. 5(a) and 5(b)), the trend of the data is indicated by the theories. The leveling off of the data at an angle of attack of 30° coincides with the movement of the flow stagnation line from the cylindrical leading edge to the slab. Typical position of the flow stagnation line on a delta wing is shown in the oil flow photographs of reference 4. In applying

8

the isolated cylinder theories, no allowance was made for this shift. The data at the $L/t = 0$ station, which may be considered as a line on a cylinder, follow the theoretical trend to higher angles of attack than at the other stations. Similarly, for the blunt-nose model (fig. 5(b)), the data at the $L/t = 0$ station, which may be considered as a line on a sphere, show good agreement with the sphere theories for angles of attack up to 40°. At the higher angles of attack there is considerable discrepancy between these data and theory.

Distributions of the heat-transfer parameter along the leading edge at various stations s_n/t are presented in figures 6 and 7. The point of maximum heating around the leading edge approximately coincides with the location of the Newtonian stagnation point. The heating decreases sharply from this maximum heating with distance around the leading edge. In general, the heating along the leading edge of the sharp-nose model is relatively constant for each of the stations s_n/t at angles of attack from 0° to 30°. (See figs. 6(a) and 6(b).) However, at an angle of attack of 30°, the heating along the juncture of the leading edge and the slab region ($s_n/t = 0.785$) decreases sharply toward the trailing edge. At the higher angles of attack (figs. 6(c) and 6(d)), the heating rate on the windward side gradually decreases with distance from the apex.

The heating along the leading edge of the blunt-nose model (fig. 7) is generally similar to that for the sharp-nose model (fig. 6). However, the leading-edge heating was higher on the blunt-nose model than on the sharp-nose model. At an angle of attack of 0° (fig. 7(a)), the data in the region of the blunt nose ($L/t < 2$) drop off and then increase slightly. This nose effect seems to have disappeared at an angle of attack of 30° (fig. 7(b)) for positive values of s_n/t and the windward heating gradually decreases toward the trailing edge. This decrease in heating is also seen at an angle of attack of 60° (fig. 7(c)) and for a portion of the leading edge at an angle of attack of 90° (fig. 7(d)). For the 90° angle-of-attack case, the Newtonian stagnation line has shifted from the leading edge to the slab region and caused an increase in the heating over the rearward portion (large values of L/t) of the leading edge.

Slab and Leading Edge

The variation of the heat-transfer parameter along lines normal to the cylindrical leading edge on the sharp-nose delta wings is presented in figure 8. The surface distance s_n/t is measured from the plane of symmetry of the leading edge; positive values indicate the windward surface and negative values, the leeward surface. The short-dashed vertical lines at $s_n/t = \pm 0.785$ on the figures indicate the juncture of the leading-edge and slab regions. The solid vertical line in the leading-edge region denotes the Newtonian stagnation point which is in close agreement with the point of peak heating as indicated by the data at all angles of attack. Also shown in this figure is the leading-edge heating distribution calculated with Lees' theory (ref. 10) for the heat-transfer distribution around a cylinder. This distribution was used with the Fay and Riddell stagnation-point value. (See eq. (2).) For the angle-of-attack range of

the tests, the data on the leading edge of the sharp-nose models followed the trend predicted by swept cylinder theory. For all angles of attack, the measured heating at each L/t station decreases with increasing distance from the leading-edge Newtonian stagnation point. With increasing angle of attack the leading-edge Newtonian stagnation point moves toward the slab and the heating on the slab approaches the maximum heating on the leading edge.

On the slab, at a given value of s_n/t, the heat transfer on the sharp-nose models (fig. 8) is higher along the wing center line (solid symbols) than on other parts of the slab surface for the angles of attack tested, except at $\alpha = 10^{\circ}$. At angles of attack up to about 20°, the heating along the center line was essentially constant for each angle of attack. For angles of attack from 30° to 60°, the center-line heating was highest in the region of the slab apex and gradually decreased toward the trailing edge. At the higher angles of attack the point of maximum heating shifts to the slab region and the center-line heating again tends to become constant at each angle of attack.

On the slab, the data are compared with laminar strip theory (ref. 11) by utilizing oblique shock relations to obtain the pressure distributions for angles of attack from 0° to 30° and Newtonian ($C_{p,max} = 2.0$) pressure distributions for the higher angles of attack. The data on the slab center line are compared with cross-flow theory obtained from the following equation of reference 1:

$$\frac{h_{cf}}{h_{0,s}} \approx \frac{\sin \alpha}{1.414} \sqrt{\left(\frac{\mu_{0,N}}{\mu_0}\right)^{0.8} \left(\frac{T_0}{T_{0,N}}\right)^{0.3} \frac{\dot{u}}{\frac{s_0}{t} - 0.285}}$$

where $\dot{u}$ was obtained from reference 1 and designates the cross-flow stagnation-point velocity gradient at a point on the center line of the wing nondimensionalized with respect to the velocity gradient at the stagnation point of a sphere.

The relatively wide variations in heating rates over the slab are such as to preclude prediction of more than the general distribution through use of the strip theory since the latter is based upon the assumption of uniform heating along rays parallel to the leading edge. The cross-flow theory at angles of attack from 40° to 60° is in excellent agreement with the measured center-line heating rates. At the higher angles of attack the theory overestimates both the magnitude of the heating rates and the variation along the chord.

The maximum heating on the leeward slab of the sharp-nose model occurs along the center line for angles of attack up to about 40°. At these angles of attack, large differences exist between the center-line data and that along the 10° ray.

Figure 9 presents the heat-transfer data for the blunt-nose models. Again the solid vertical line in the leading-edge region indicates the Newtonian stagnation point and shows good agreement with the measured data. Lees' theories

10

for the heat-transfer distribution around a cylinder and a sphere are shown to encompass the measured leading-edge data for angles of attack up to 30°. (See fig. 9(e).) At the higher angles of attack the theories tend to coincide and overestimate the data although they closely predict the gradients around the cylinder. The data at the $L/t = 0$ station show good agreement with the sphere theory throughout the angle-of-attack range.

At angles of attack other than 10°, 20°, and 30°, the heat transfer at given values of s_n/t is higher along the center line than on other parts of the surface. Exception to this trend is similar to that observed on the sharp-nose model at an angle of attack of 10° but in contrast to previous tests (ref. 1) where the center-line heating rates were consistently higher than those over the remainder of the slab. The center-line heating decreases in the direction of the trailing edge for most of the angles of attack tested. At an angle of attack of 30° (figs. 9(d) and 9(e)), a sharp rise in the center-line heating occurs on both blunt-nose models and suggests transition in a very small region at the trailing edge. However, because of the higher local Reynolds numbers, transition would be expected on the sharp-nose model first and is not indicated in these tests. A similar increase in the center-line heating is also seen at angles of attack of 70° and 90°. (See figs. 9(i) and 9(k).) Areas of agreement of data with strip theory and cross-flow theory at these angles of attack must be considered fortuitous as the theory and experiment at other attitudes differ by as much as 2 to 1.

On the leeward slab of the blunt-nose model, the center-line heating, indicated by the solid symbols, is considerably higher than the off-center data at angles of attack below about 50°, but at higher angles of attack, the heating generally decreases toward the center line. The heat-transfer rate for the sharp- and blunt-nose models is presented in figure 10 as a function of surface distance along the wing center line. The increase in heating rate with increasing angle of attack on both the sharp- and blunt-nose models is consistent with theory although marked deviations in both magnitude and distribution are noted under many conditions. On the sharp-nose model (fig. 10(a)), the heating on the windward surface tends to level off toward the trailing edge and becomes constant at each angle of attack. Repeat runs verified the overlap of the data shown at angles of attack of 0° and 10°. Cross-flow theory as previously noted agrees well with the measured center-line data at $\alpha \geqq 40°$.

The leeward data on the sharp-nose model (fig. 10(a)) is indicative of uniform heating for angles of attack up to 20°. At $\alpha \lesssim 30°$ a sharp decrease in the heating occurs toward the trailing edge; this change may be influenced by sting and adapter effects.

The measured heating along the center line of the blunt-nose models is presented in figure 10(b). In general, the heating on the windward slab decreases in the direction of the trailing edge at each angle of attack tested except at angles of attack of 30°, 70°, and 90°. The data show fair agreement with strip theory at an angle of attack of 0° but are below the prediction of strip theory at the higher angles. In general, cross-flow theory overestimates the measured data; however, in the region of the juncture of the nose and the slab, fair agreement is shown. Comparison of figures 10(a) and 10(b) shows a

11

marked reduction in heating rates over the aft section of the wing at angles of attack less than 40° as a result of nose blunting. At higher angles of attack no significant change was observed. The large reduction in heating with the nose blunted is confined to a region close to the center line.

On the leeward slab, the heating rate at angles of attack of 10° and 20° is greater than that at an angle of attack of 0°. The heating distributions on the leeward surface divide themselves into two distinct groups based on angle of attack. (See fig. 10(b).) These groupings cannot be attributed to model differences in view of the very good agreement indicated at the overlapping angle of attack (30°). The leeward heating rates are an order of magnitude less than the windward values at $\alpha = 30°$ and two orders lower as the angle of attack approaches 90°.

CONCLUSIONS

Heat-transfer distributions have been presented for 70° swept slab delta wings at a Mach number of 9.86 and angles of attack up to 90°. These wings had cylindrical leading edges and either a sharp or a blunt nose. The results of the investigation indicate the following conclusions:

1. Lees' theory for the heat-transfer distribution is shown to be in good agreement with the data obtained on the nose and leading edge.

2. The point of peak heating on the leading edge is in close agreement with the Newtonian stagnation point.

3. The heating rates on the leeward slab at angles of attack from 20° to 30° are an order of magnitude less than the windward values and differ by two orders as the angle of attack approaches 90°.

4. Scattered agreement of experimental data with strip theory was shown at low angles of attack.

5. Cross-flow theory was in excellent agreement with experimental data on the center line at angles of attack from 40° to 60°; however, at other model attitudes the theory differed significantly from experiment.

6. Nose blunting resulted in a reduction of heating rates over the aft center-line section of the wing at angles of attack less than about 40°. No significant change was shown at higher angles of attack.

Langley Research Center,
    National Aeronautics and Space Administration,
        Langley Station, Hampton, Va., July 8, 1964.

REFERENCES

1. Bertram, Mitchel H., and Everhart, Philip E.: An Experimental Study of the Pressure and Heat-Transfer Distribution on a 70° Sweep Slab Delta Wing in Hypersonic Flow. NASA TR R-153, 1963.

2. Jones, Robert A., and Trimpi, Robert L.: Heat-Transfer and Pressure Distributions at a Mach Number of 6 for 70° Swept Slab Wings With Sharp and Spherical Noses and Cylindrical Leading Edges. NASA TM X-682, 1962.

3. Bertram, Mitchel H., and Henderson, Arthur, Jr.: Recent Hypersonic Studies of Wings and Bodies. ARS Jour., vol. 31, no. 8, Aug. 1961, pp. 1129-1139.

4. Bernot, Peter T.: Pressure Distributions on Blunt Delta Wings at Angles of Attack up to 90° and Mach Number of 6.85. NASA TN D-1954, 1963.

5. Mueller, James N. (With Appendix by Eugene S. Love): Pressure Distributions on Blunt Delta Wings at a Mach Number of 2.91 and Angles of Attack up to 90°. NASA TM X-623, 1962.

6. Goldberg, Theodore J., and Hondros, James G.: Pressure Distributions on a Flat-Plate Delta Wing Swept 65° at a Mach Number of 5.97 at Angles of Attack From 65° to 115° and Angles of Roll From 0° to 25° at a 90° Angle of Attack. NASA TM X-702, 1962.

7. Bertram, Mitchel H., Feller, William V., and Dunavant, James C.: Flow Fields, Pressure Distributions, and Heat Transfer for Delta Wings at Hypersonic Speeds. NASA TM X-316, 1960.

8. Dunavant, James C.: Investigation of Heat Transfer and Pressures on Highly Swept Flat and Dihedraled Delta Wings at Mach Numbers of 6.8 and 9.6 and Angles of Attack to 90°. NASA TM X-688, 1962.

9. Wallace, A. R., and Little, H. R.: Heat-Transfer and Pressure Distribution on Two Delta Wing Configurations at Mach Number 20. AEDC-TDR-63-114 (Contract No. AF 40(600)-1000), Arnold Eng. Dev. Center, July 1963.

10. Lees, Lester: Laminar Heat Transfer Over Blunt-Nosed Bodies at Hypersonic Flight Speeds. Jet Propulsion, vol. 26, no. 4, Apr. 1956, pp. 259-269, 274.

11. Bertram, Mitchel H., and Feller, William V.: A Simple Method for Determining Heat Transfer, Skin Friction, and Boundary-Layer Thickness for Hypersonic Laminar Boundary-Layer Flows in a Pressure Gradient. NASA MEMO 5-24-59L, 1959.
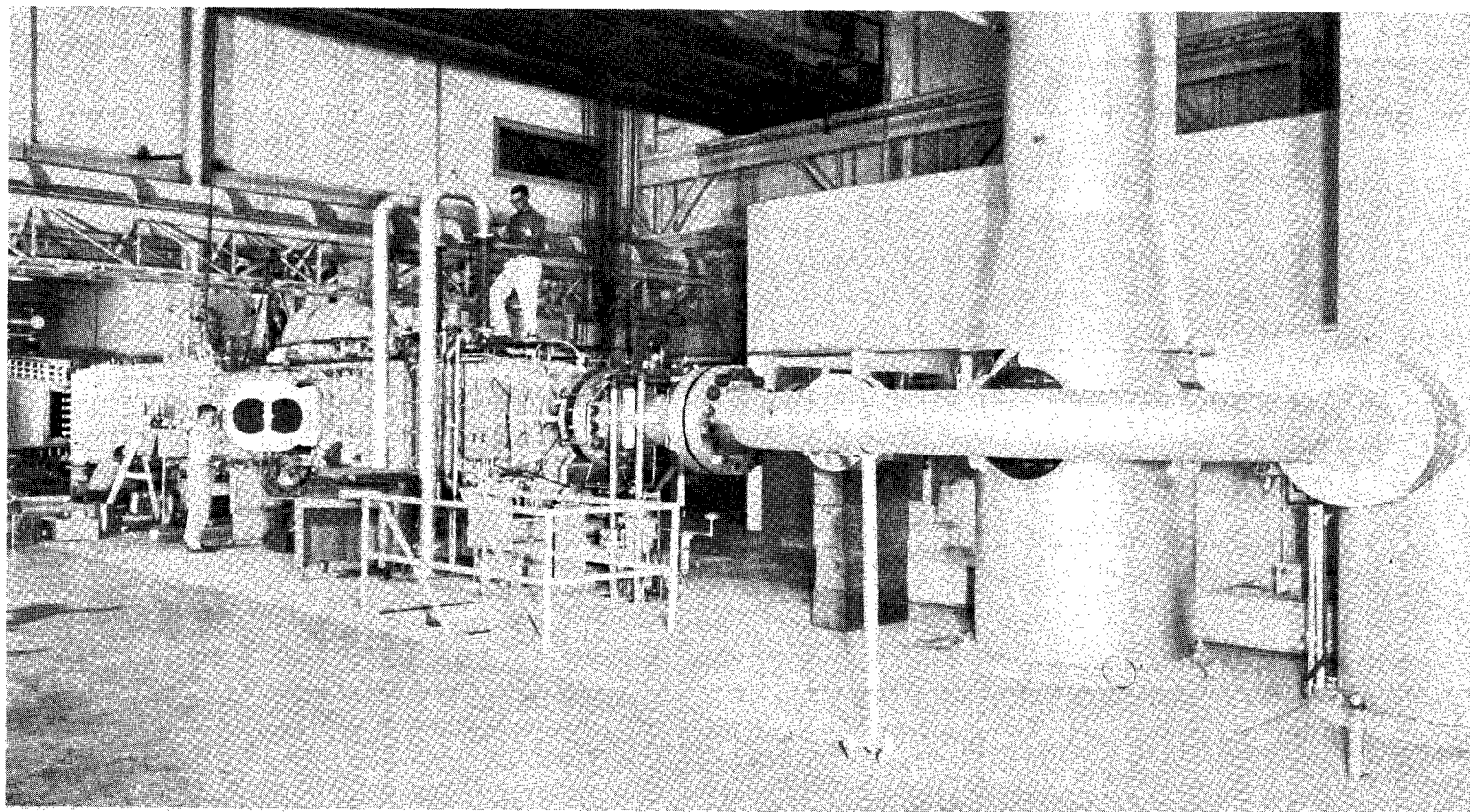
(a) General view.

L-62-7606

Figure 1.- Langley continuous-flow hypersonic tunnel.
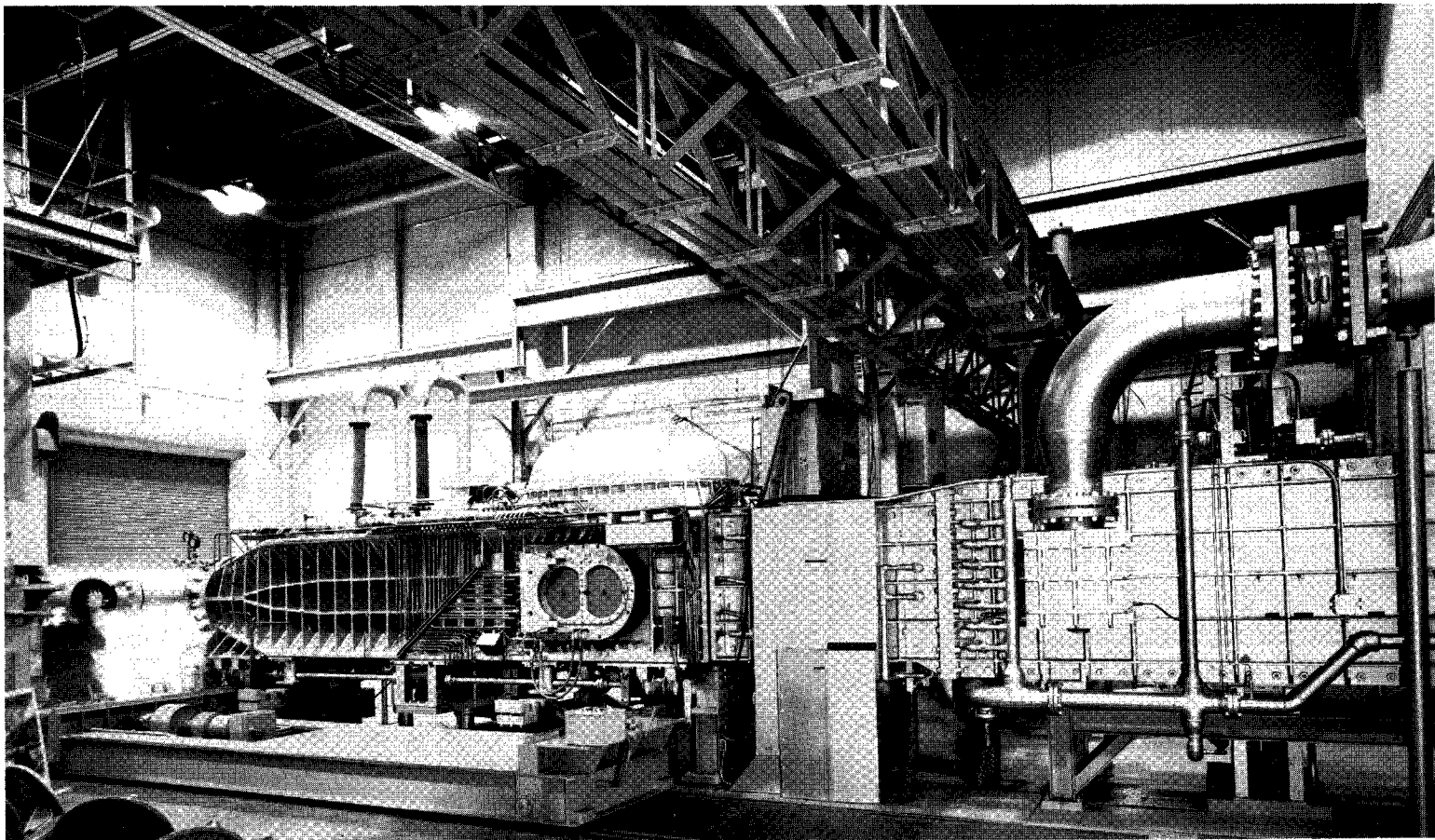
(b) Test section.

L-62-3570

Figure 1.- Concluded.
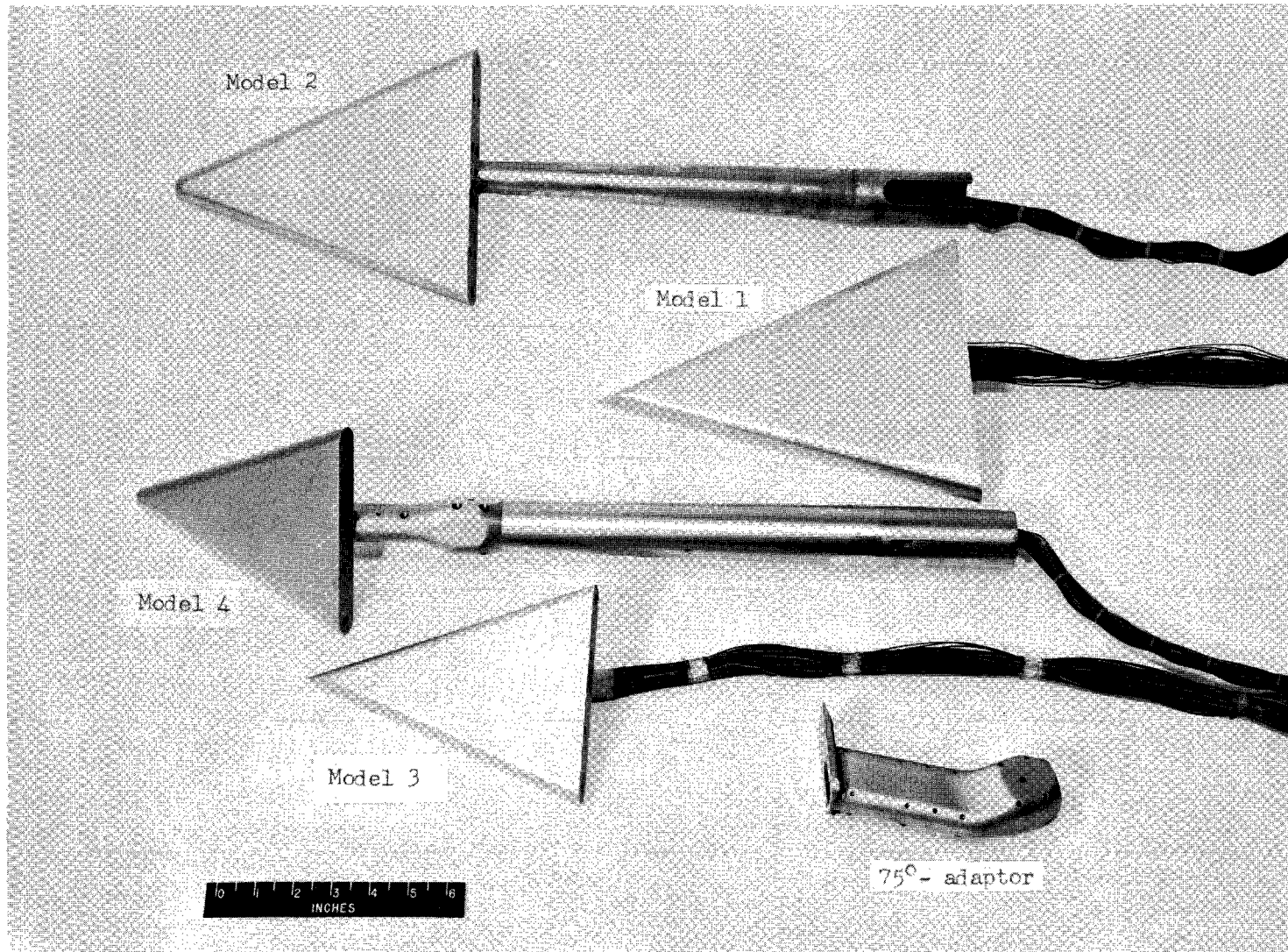
(a) Photograph of models.

L-63-9592.1

Figure 2.- Heat-transfer models.
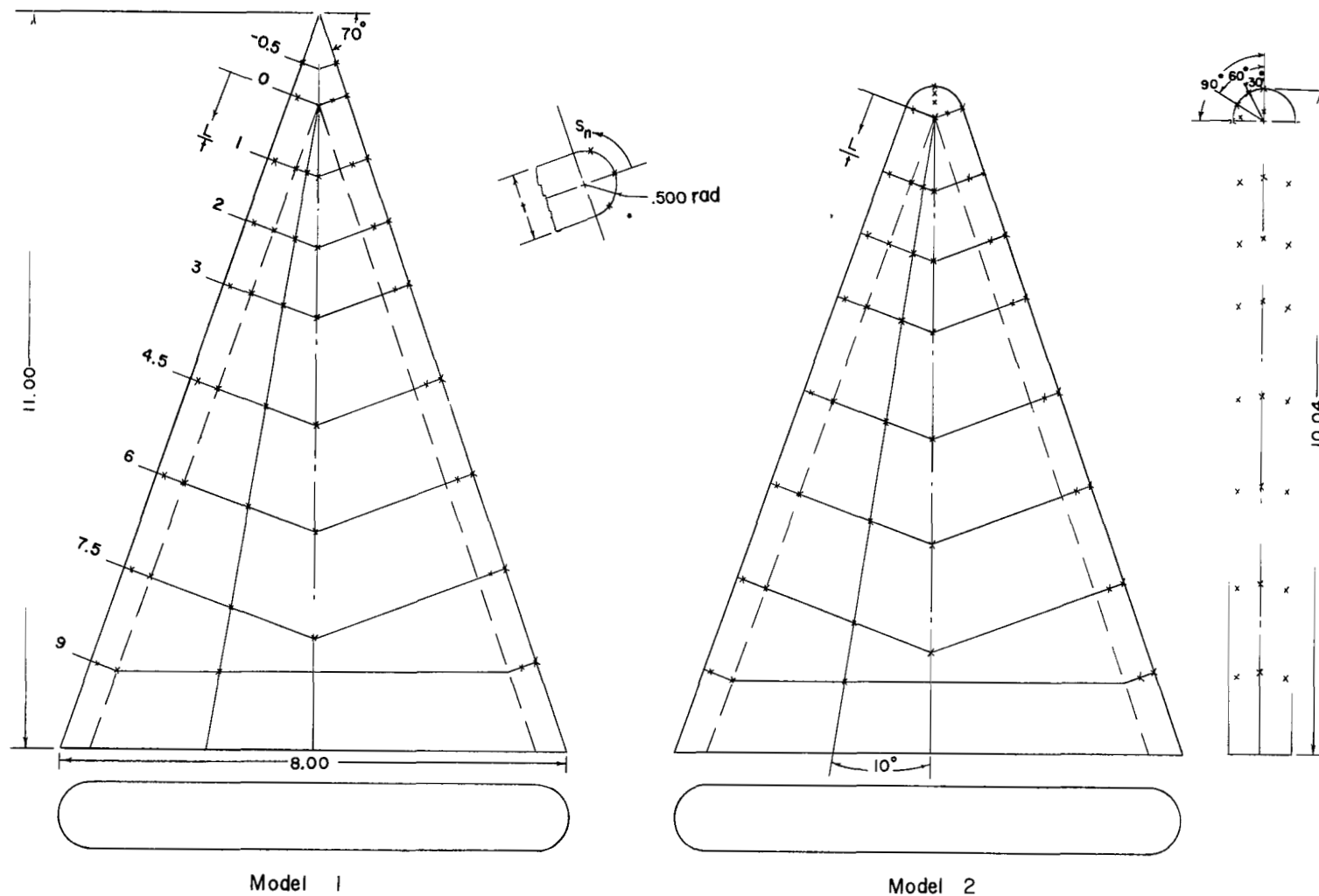
(b) Sketch of low angle-of-attack models. All dimensions are in inches.

Figure 2.- Continued.
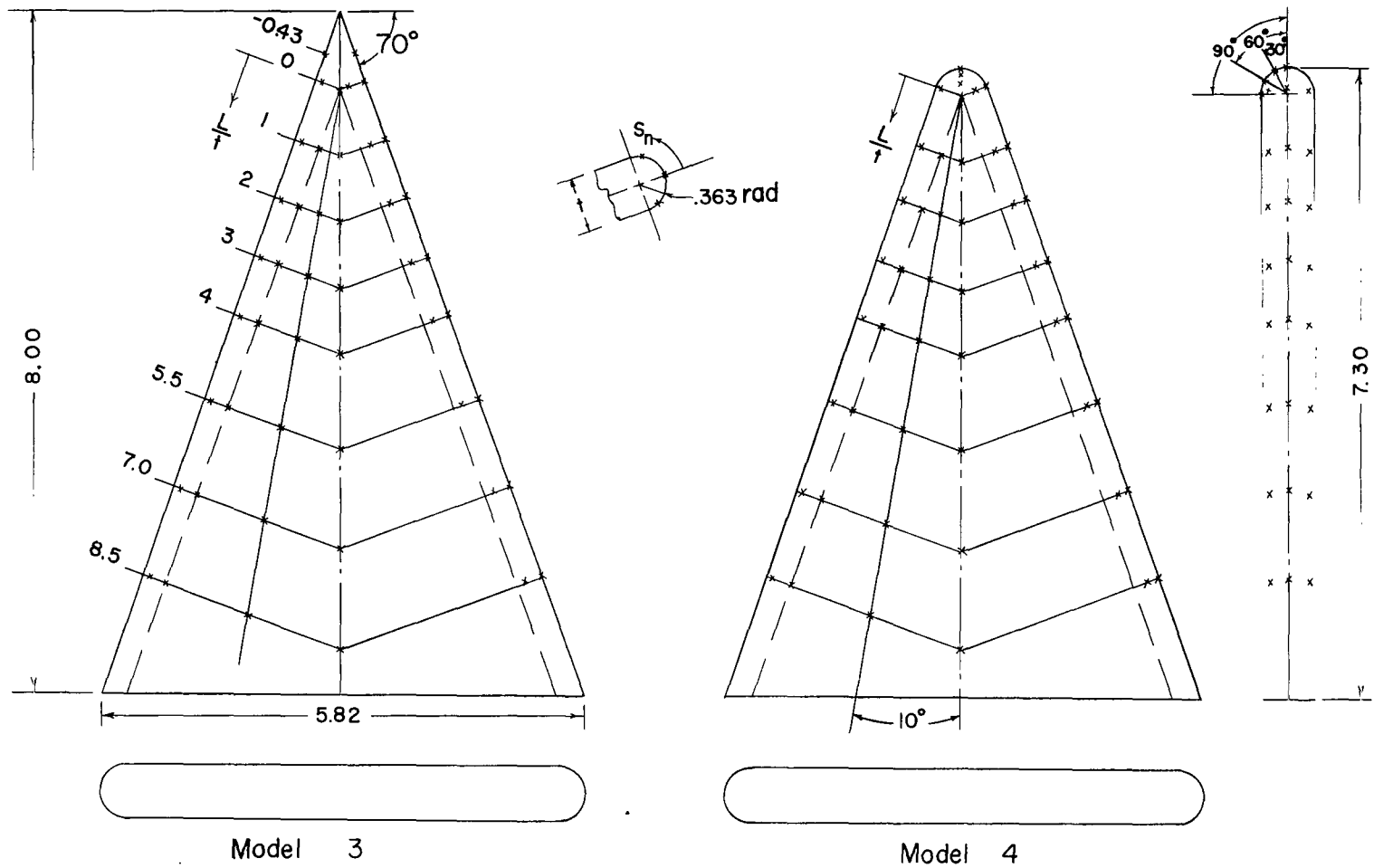
(c) Sketch of high angle-of-attack models. All dimensions are in inches.

Figure 2.- Concluded.

.072 ─── ─.500 rad

.468 rad ───

.040 ── ── .008 ── .040

.025 ──

Section B-B

.040

Juncture of nose and slab

.500 rad ─

.090

.125 ──

.007

.468 rad ─

Section A-A

Juncture of nose and leading edge

B

.072

.468 rad ─

.500 rad ─

A

B

.125

.090

A

1.050
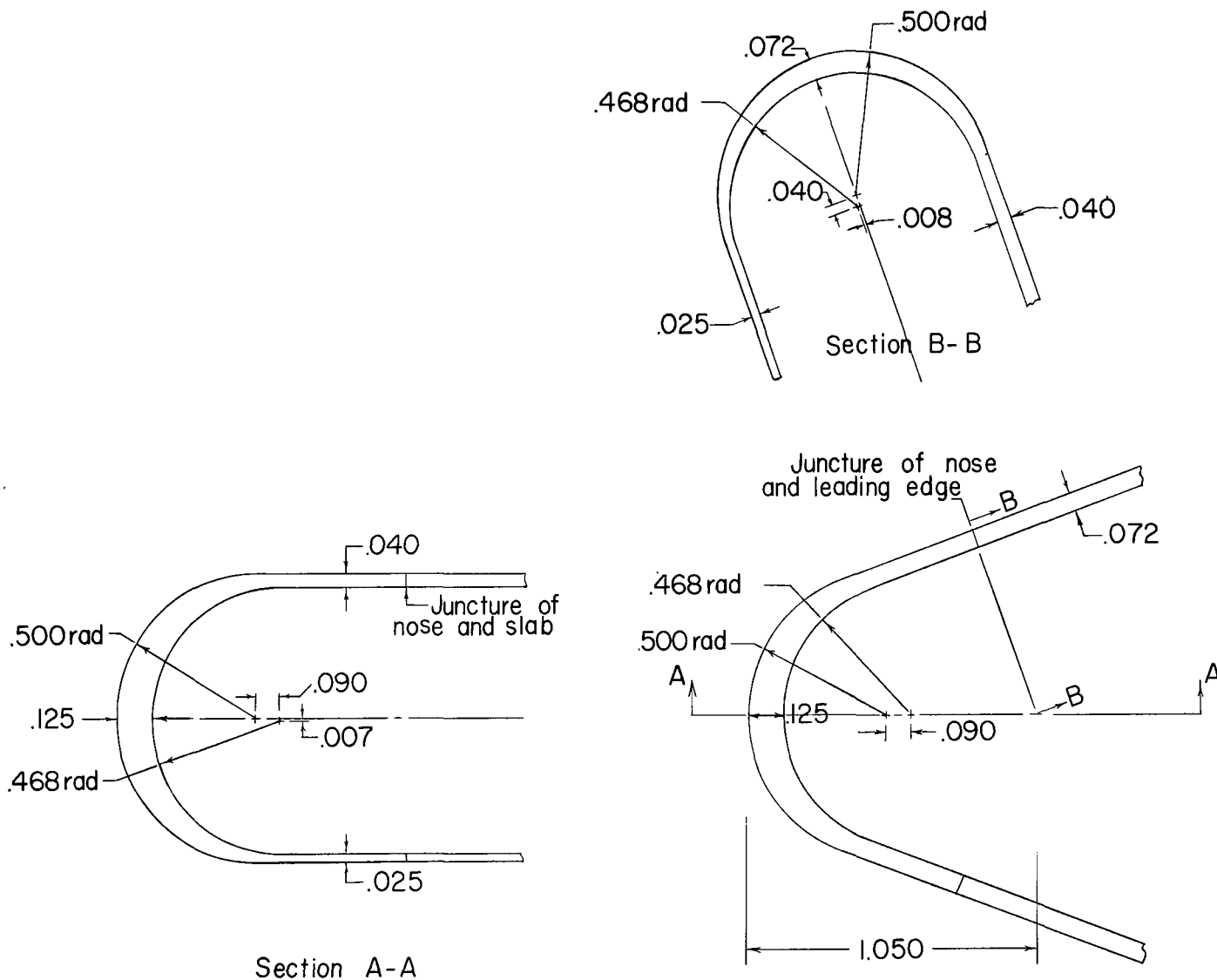
(a) Low angle-of-attack models.

Figure 3.- Variation of skin thickness over the spherical nose and blunt leading edges. All dimensions are in inches.

Section B-B

Section A - A
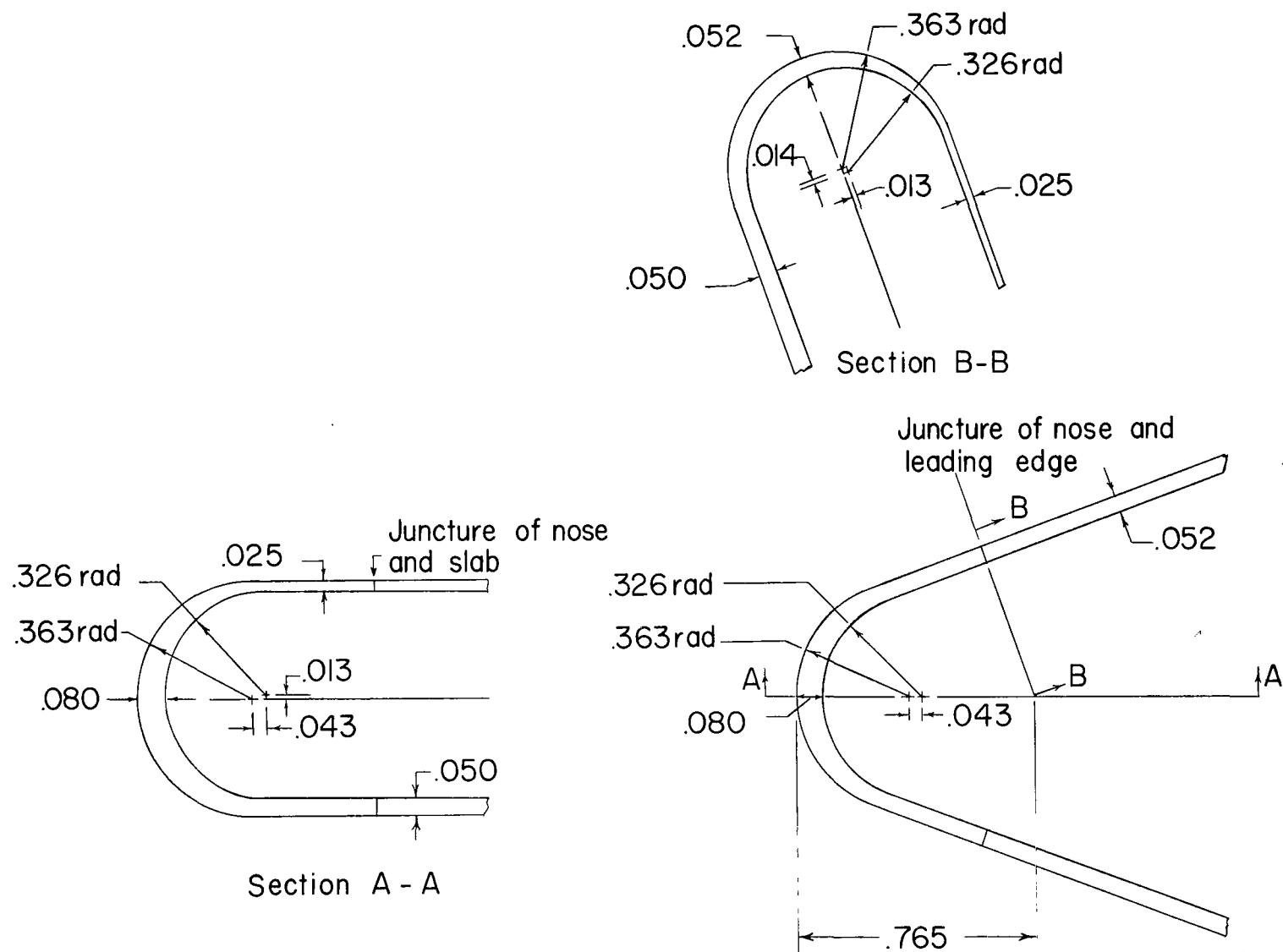
(b) High angle-of-attack models.

Figure 3.- Concluded.
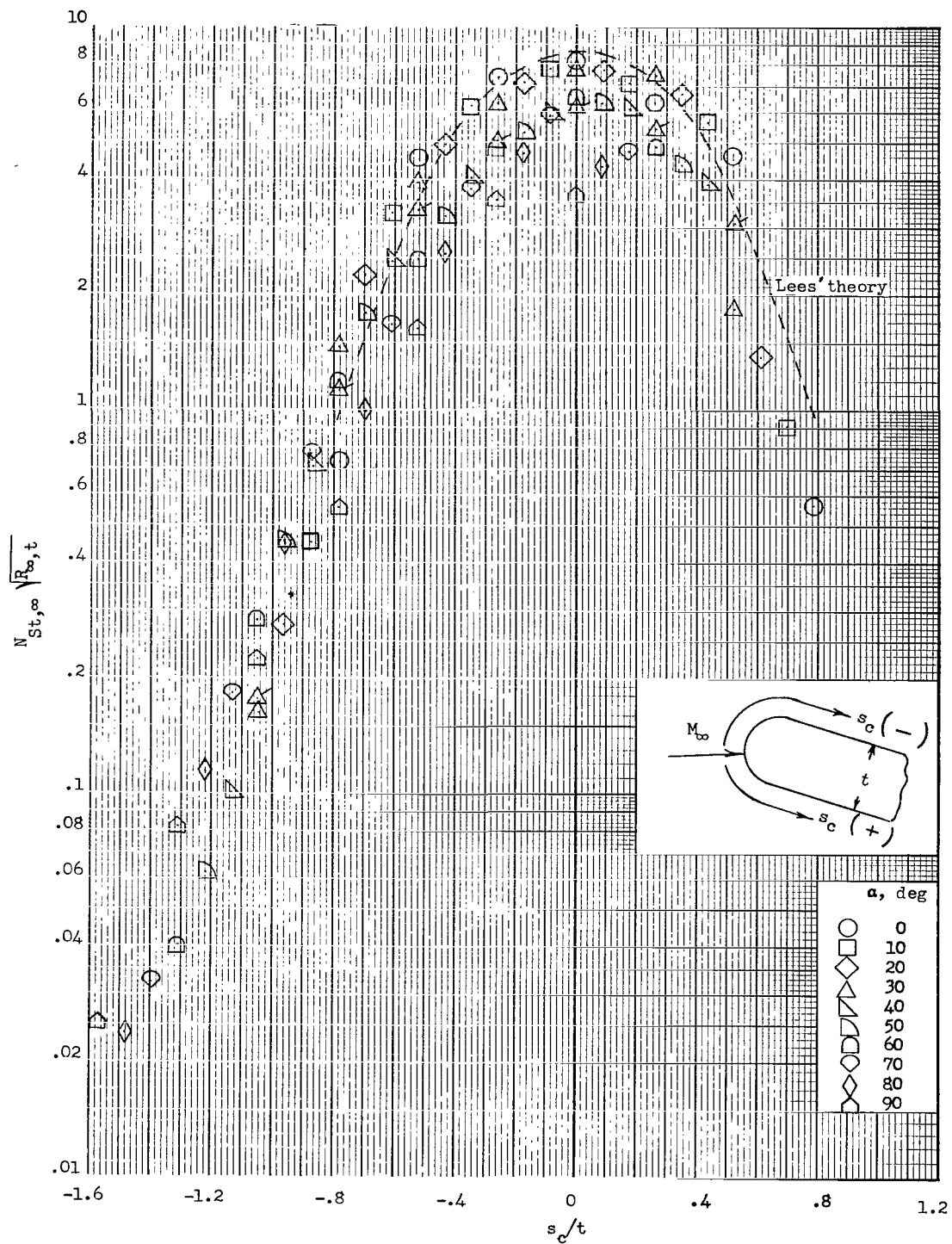
Figure 4.- Stanton number distribution on spherical nose of slab delta wing.

(a) Sharp nose.

(b) Blunt nose.
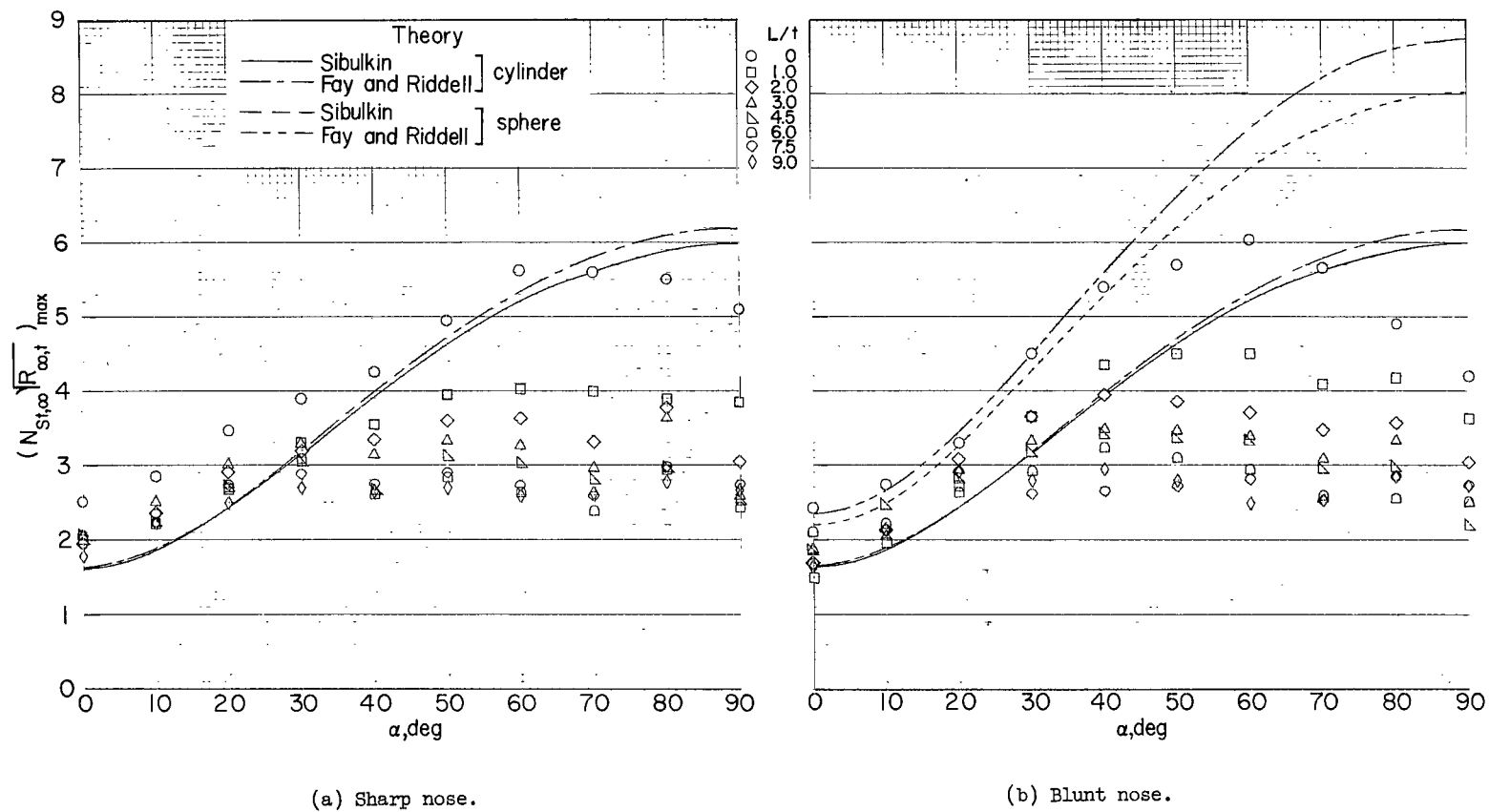
Figure 5.- Maximum Stanton number measured along the leading edge of delta wings.

(a) α = 0°.
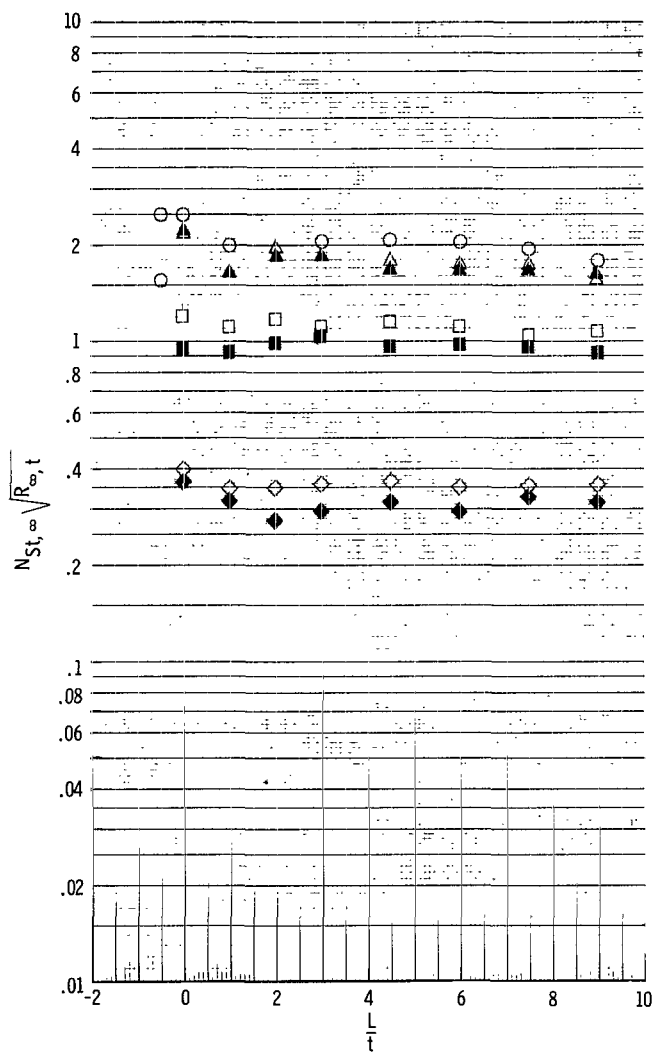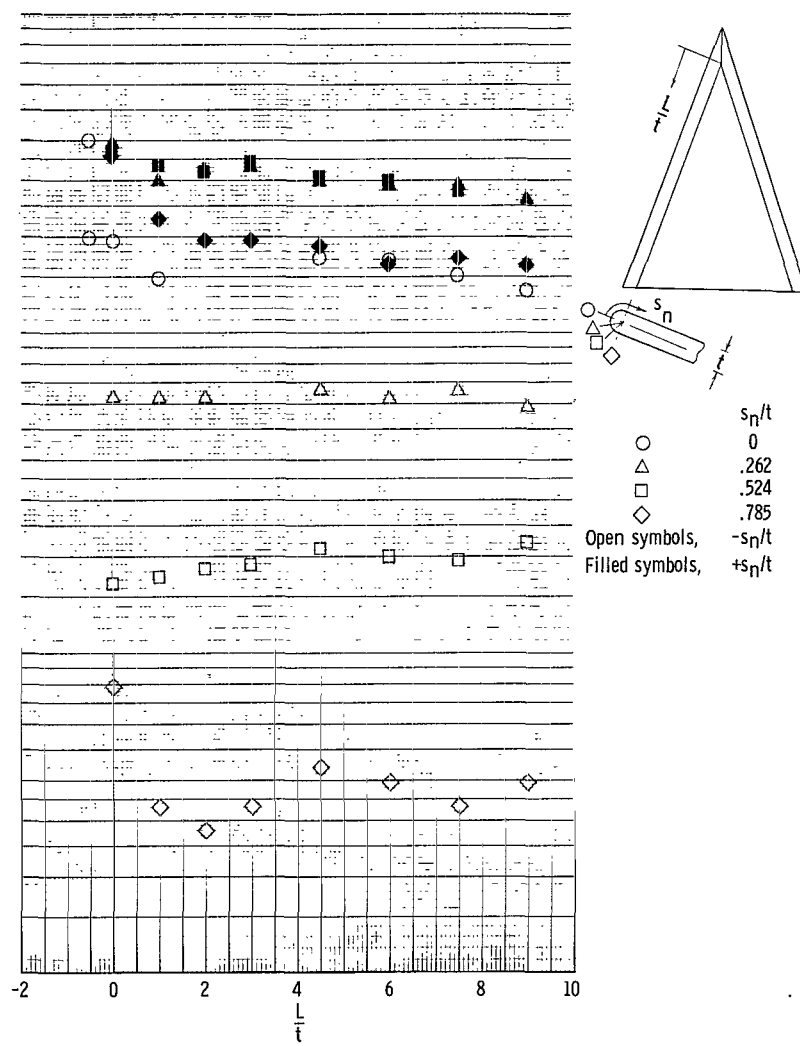
(b) α = 30°.

Figure 6.- Stanton number distribution along the leading edge at various stations normal to the leading edge. Sharp-nose model.
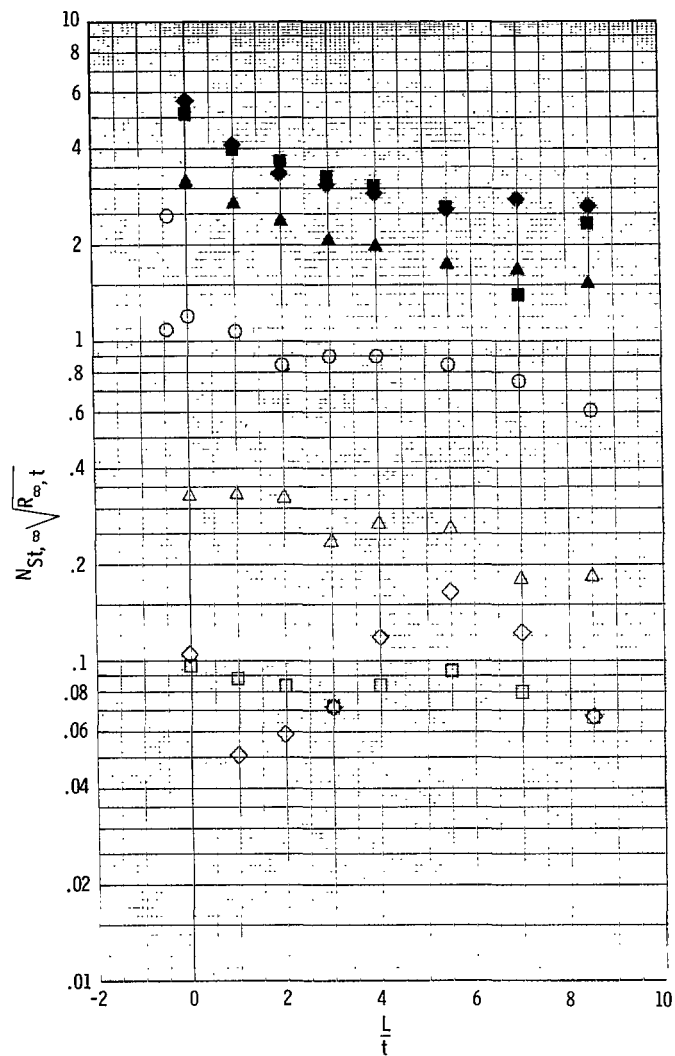
(c) $\alpha = 60^{\circ}$.
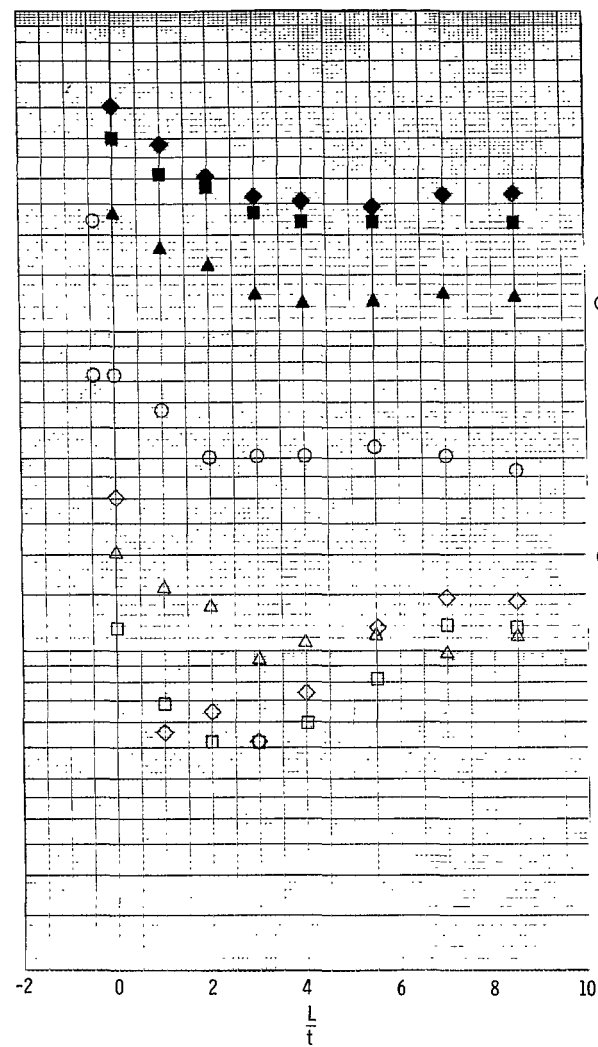
(d) $\alpha = 90^{\circ}$.
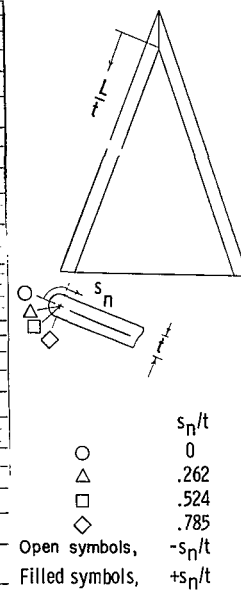
Figure 6.- Concluded.
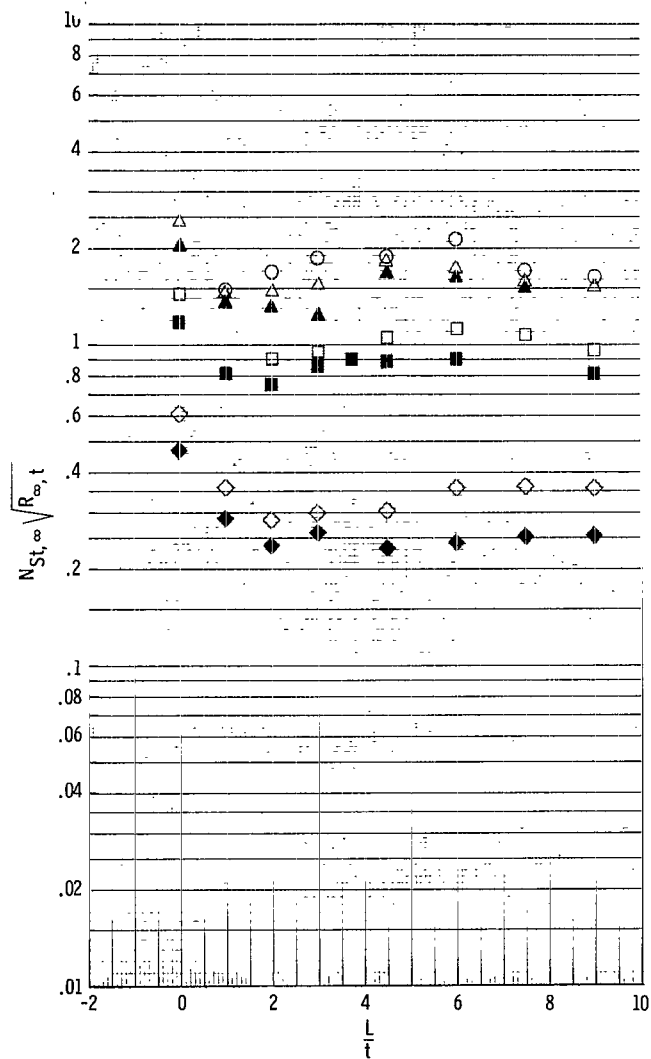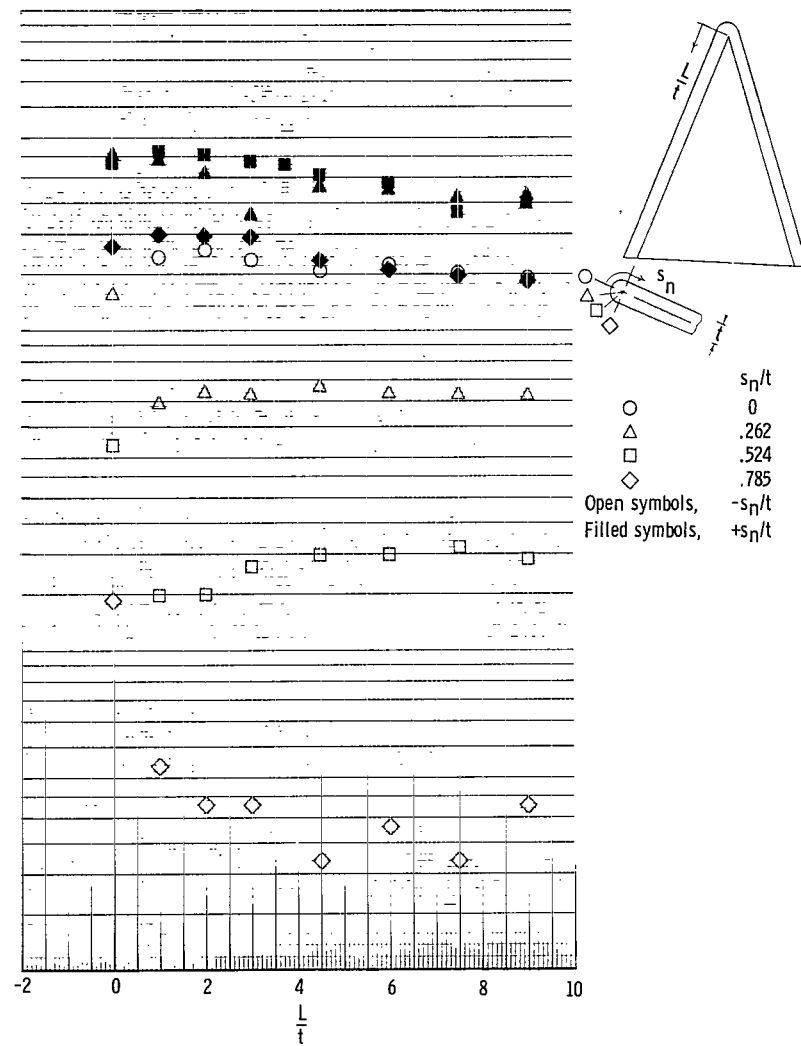
(a) α = 0°.   (b) α = 30°.

Figure 7.- Stanton number distribution along the leading edge at various stations normal to the leading edge.
Blunt-nose models.

(c) α = 60°.
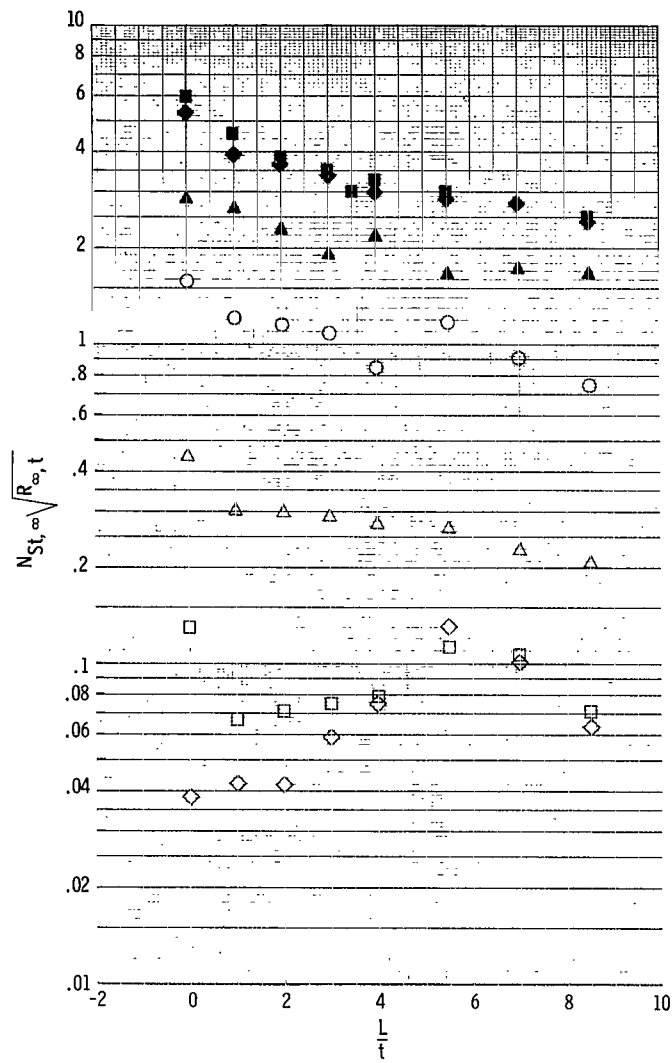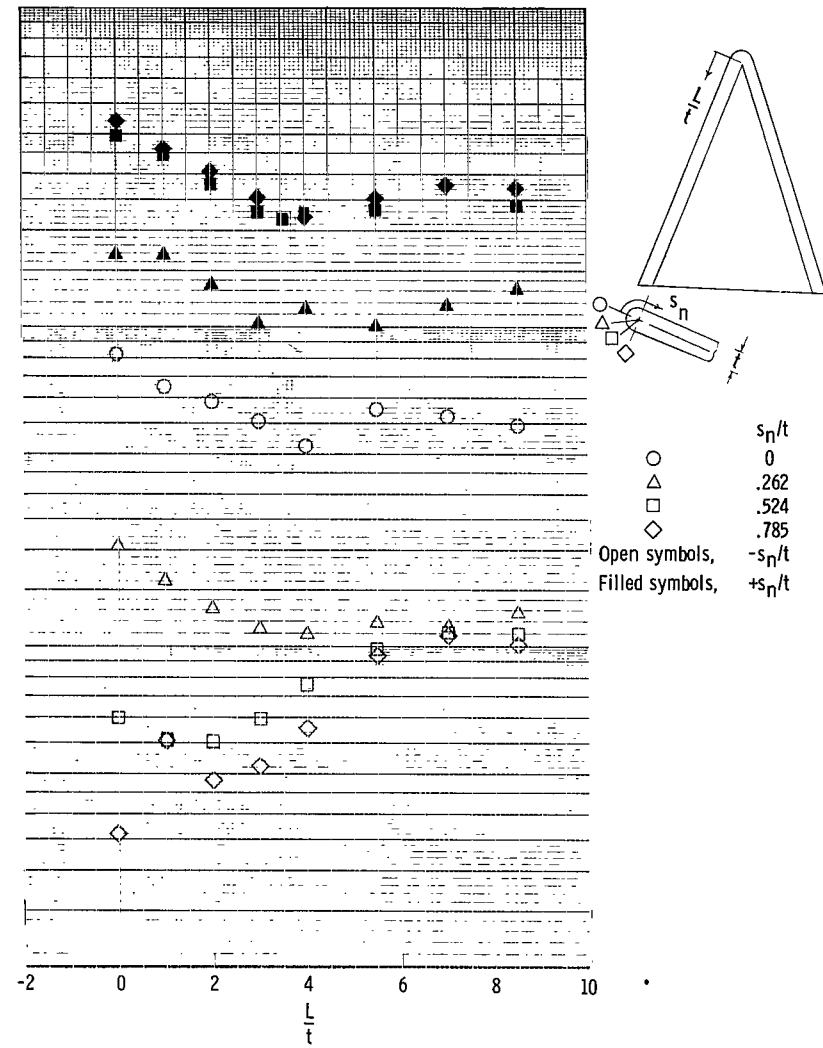
(d) α = 90°.

Figure 7.- Concluded.
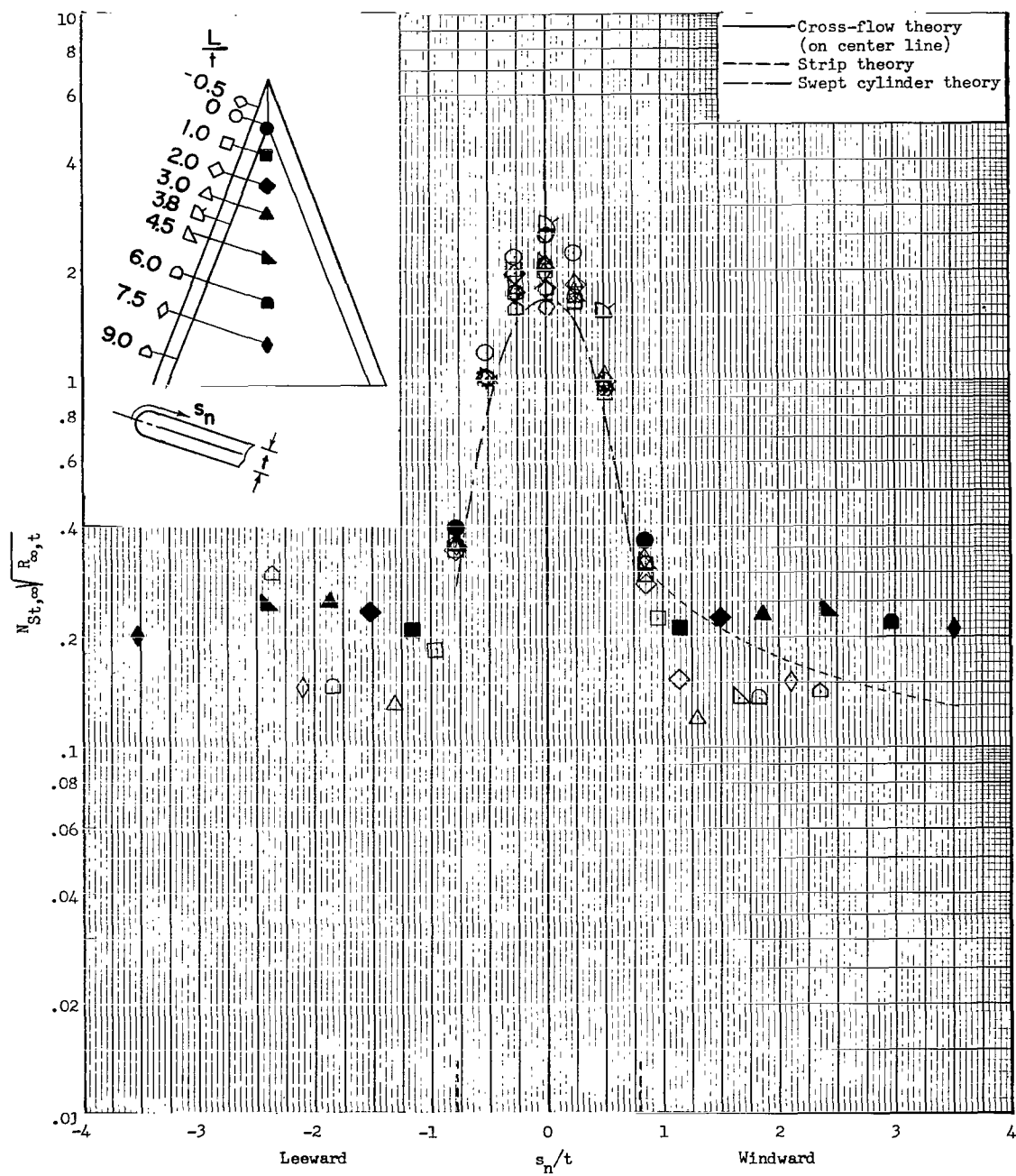
(a) α = 0°.

Figure 8.- Stanton number distribution normal to the leading edge on sharp-nose delta wing at various stations along the leading edge. Dashed vertical lines indicate juncture of leading edge and slab regions.
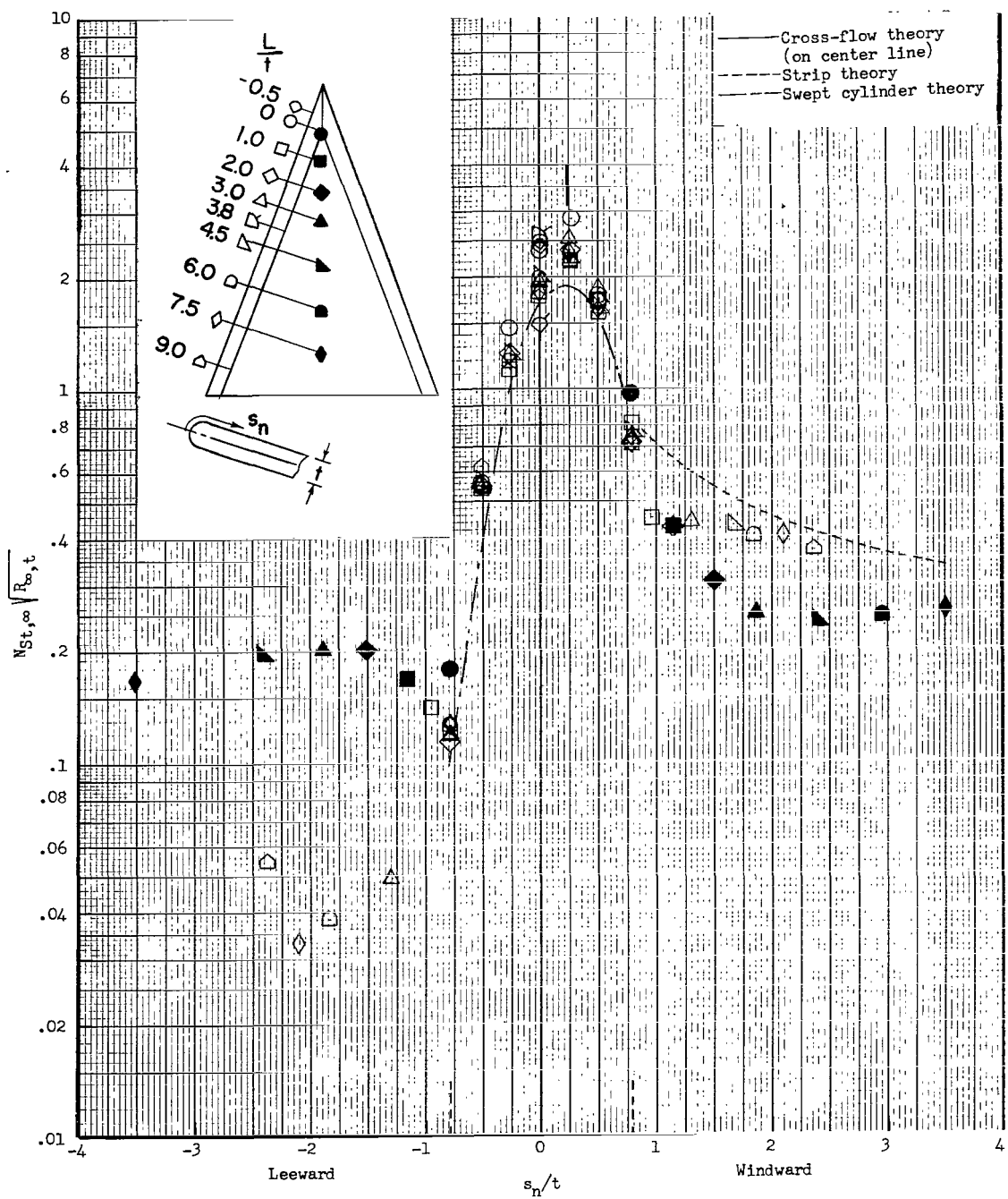
(b) $\alpha = 10°$.
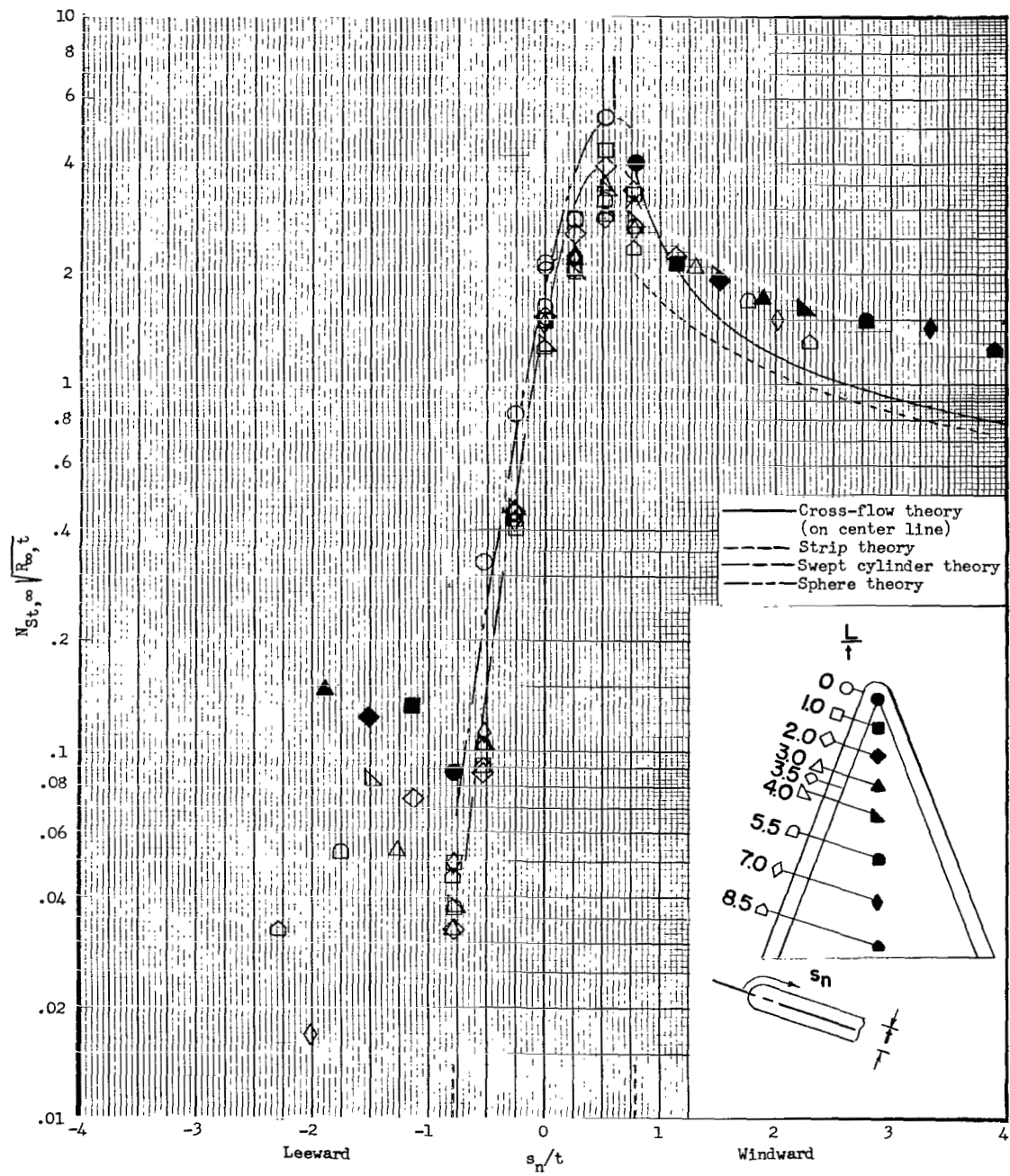
Figure 8.- Continued.
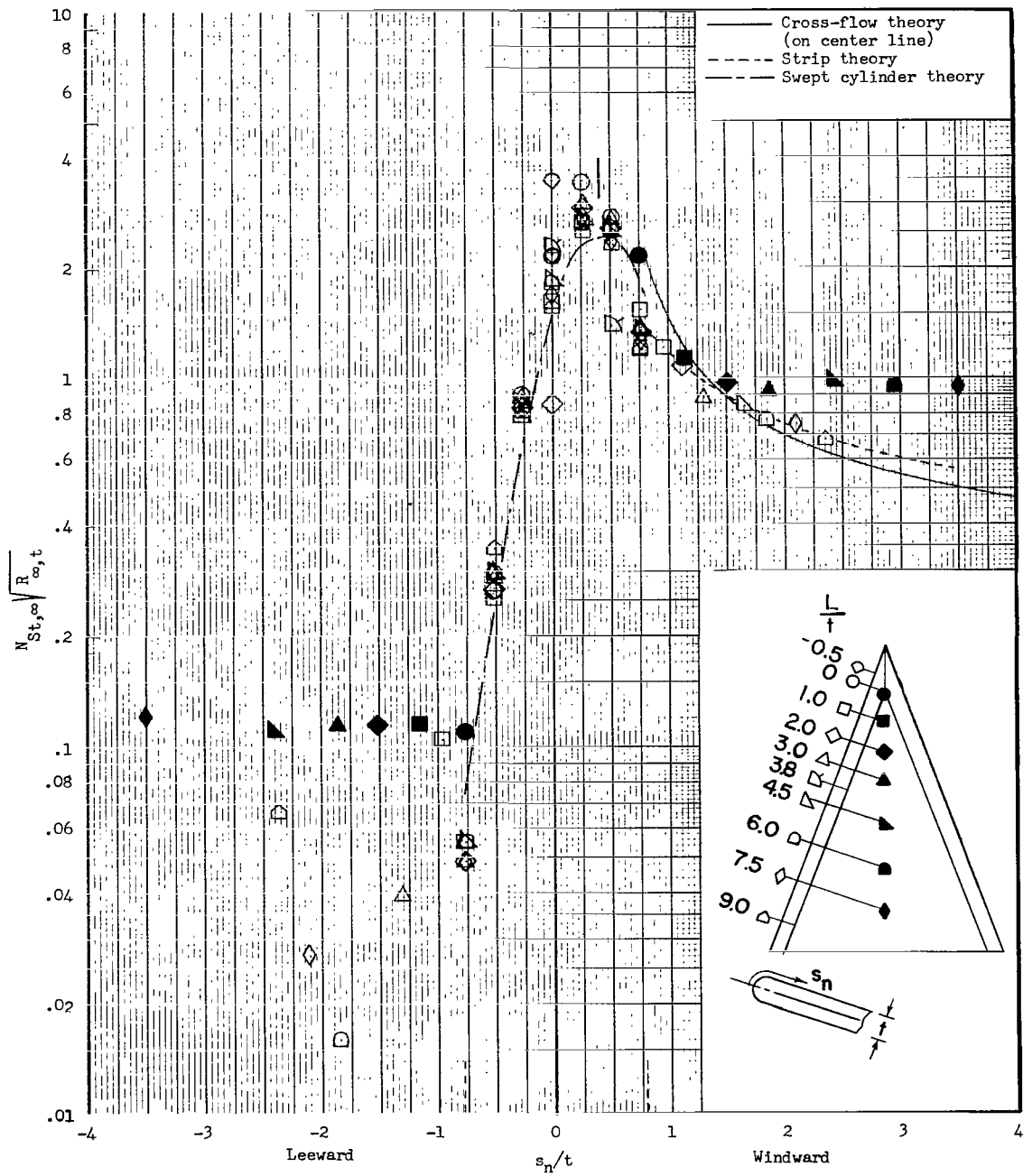
(c) α = 20°.

Figure 8.- Continued.
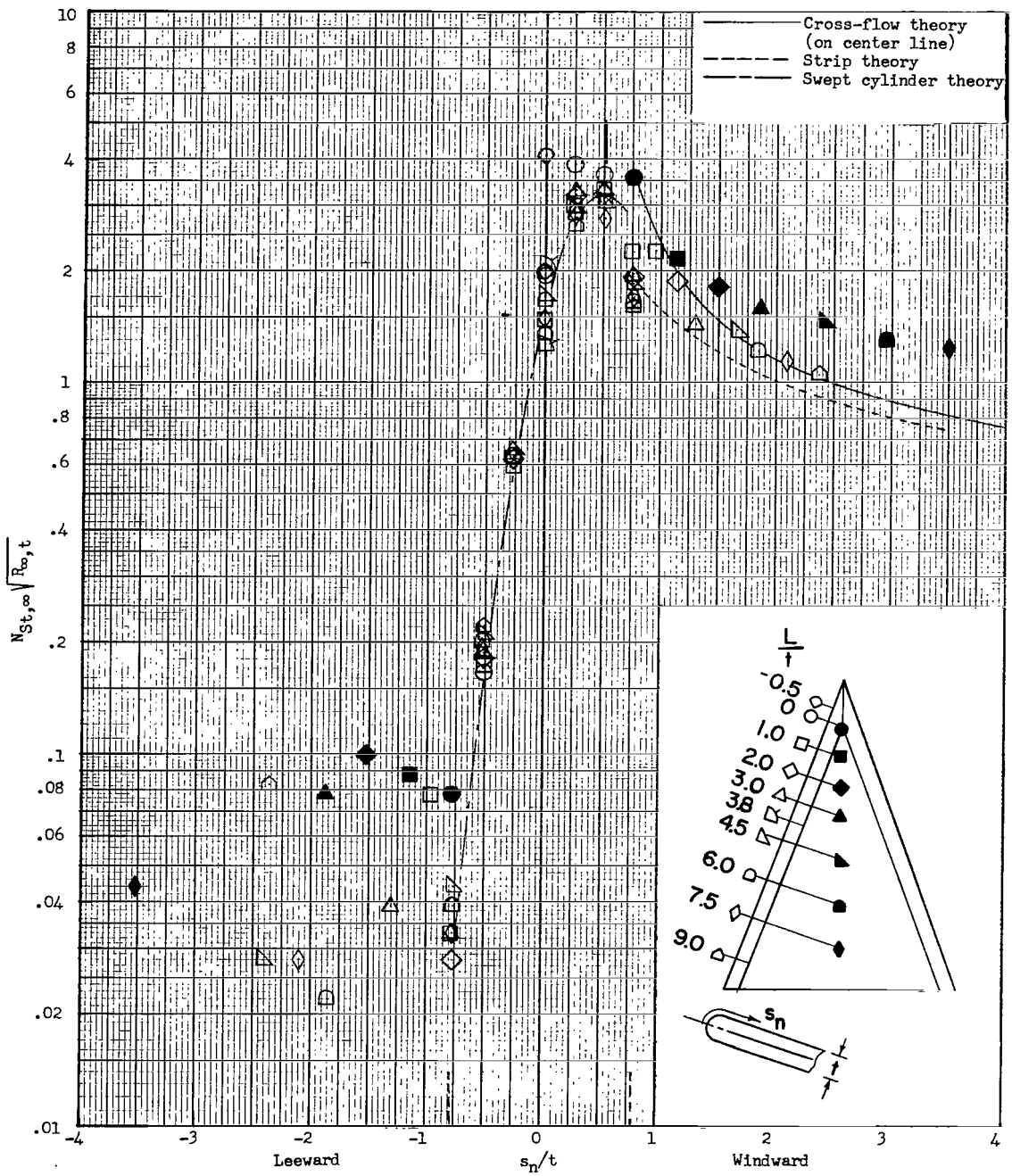
(d) $\alpha = 30^\circ$; model 1.

Figure 8.- Continued.
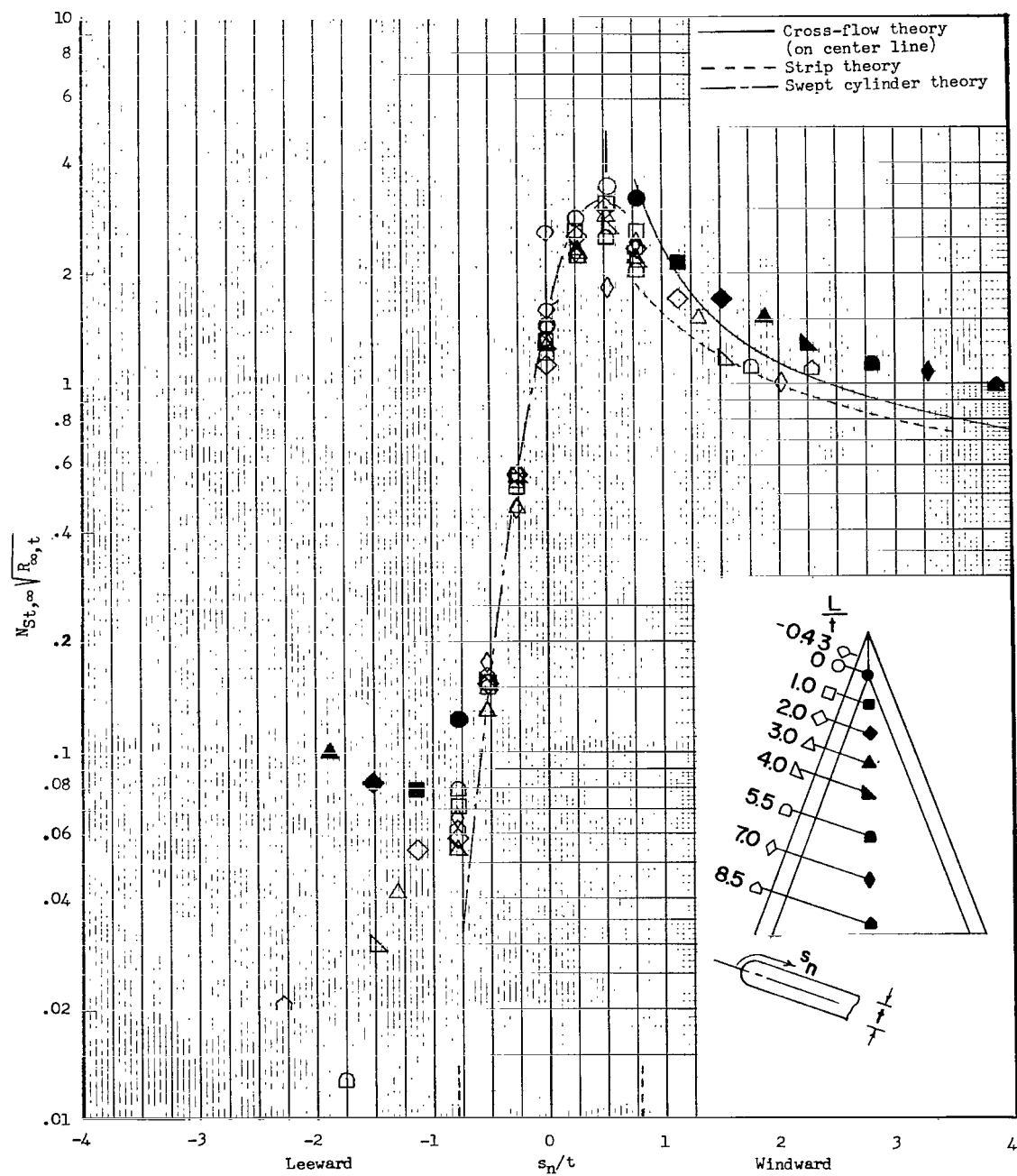
(e) $\alpha = 30°$; model 3.

Figure 8.- Continued.
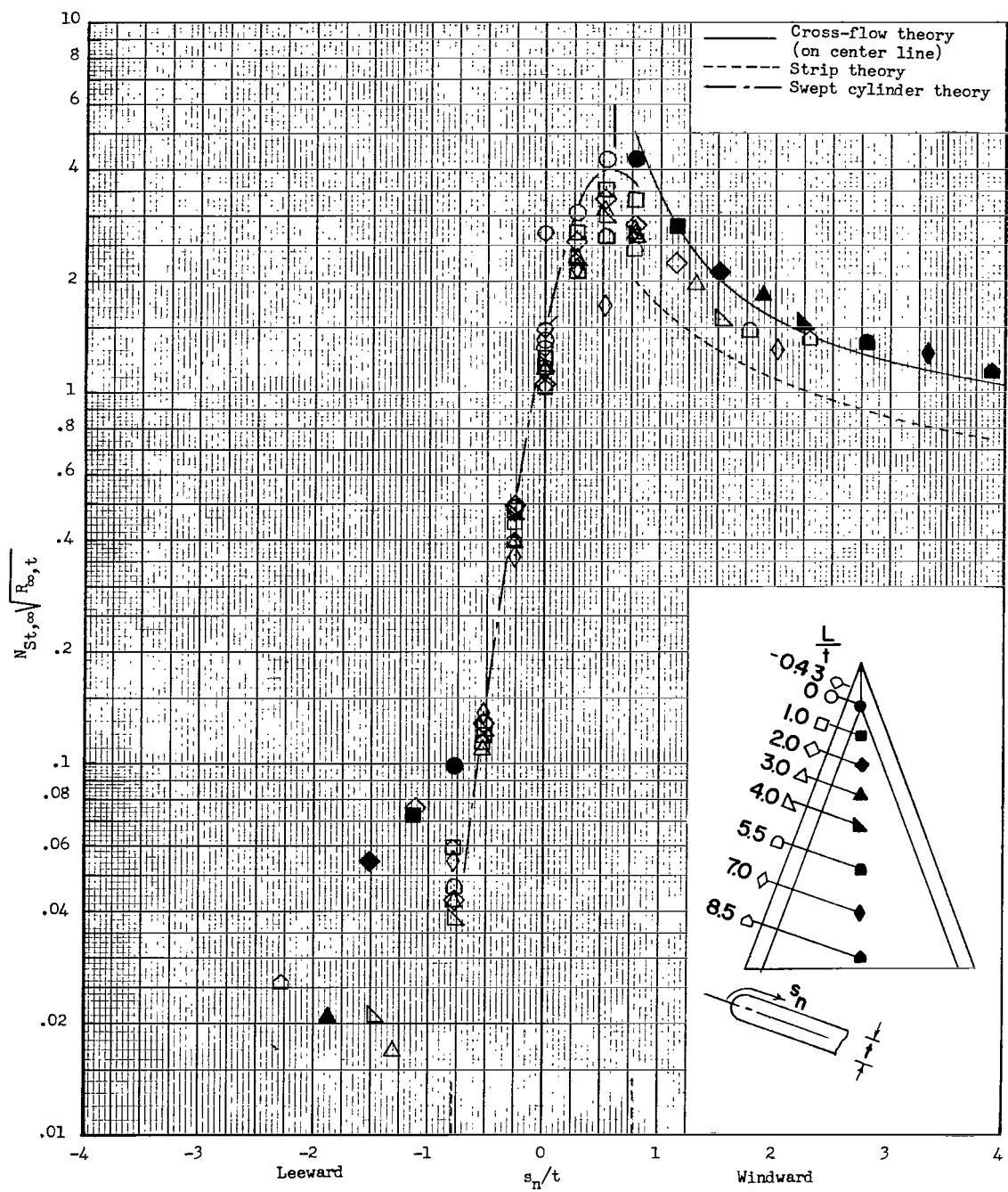
(f) $\alpha = 40°$.

Figure 8.- Continued.

(g) $\alpha = 50^o$.
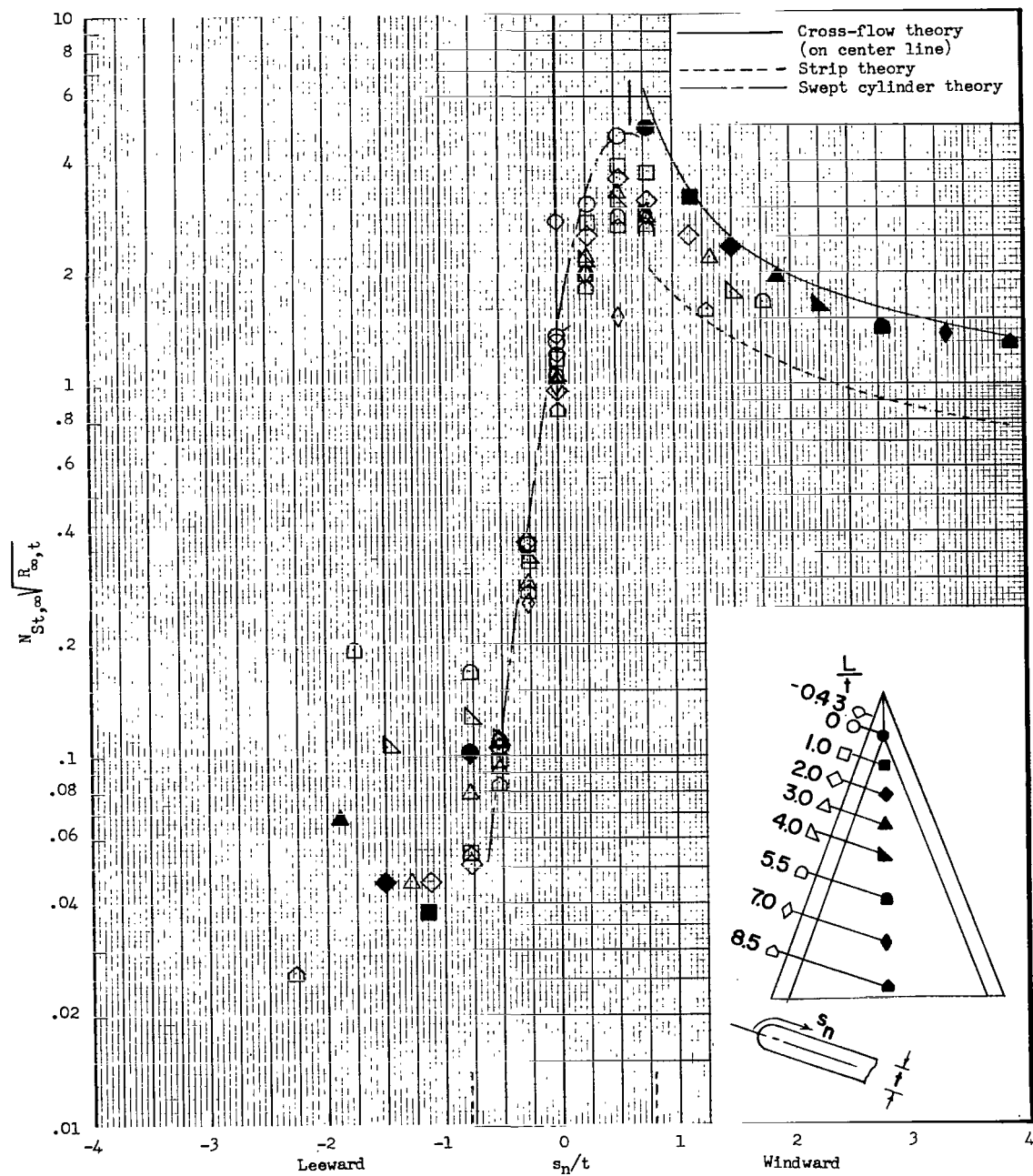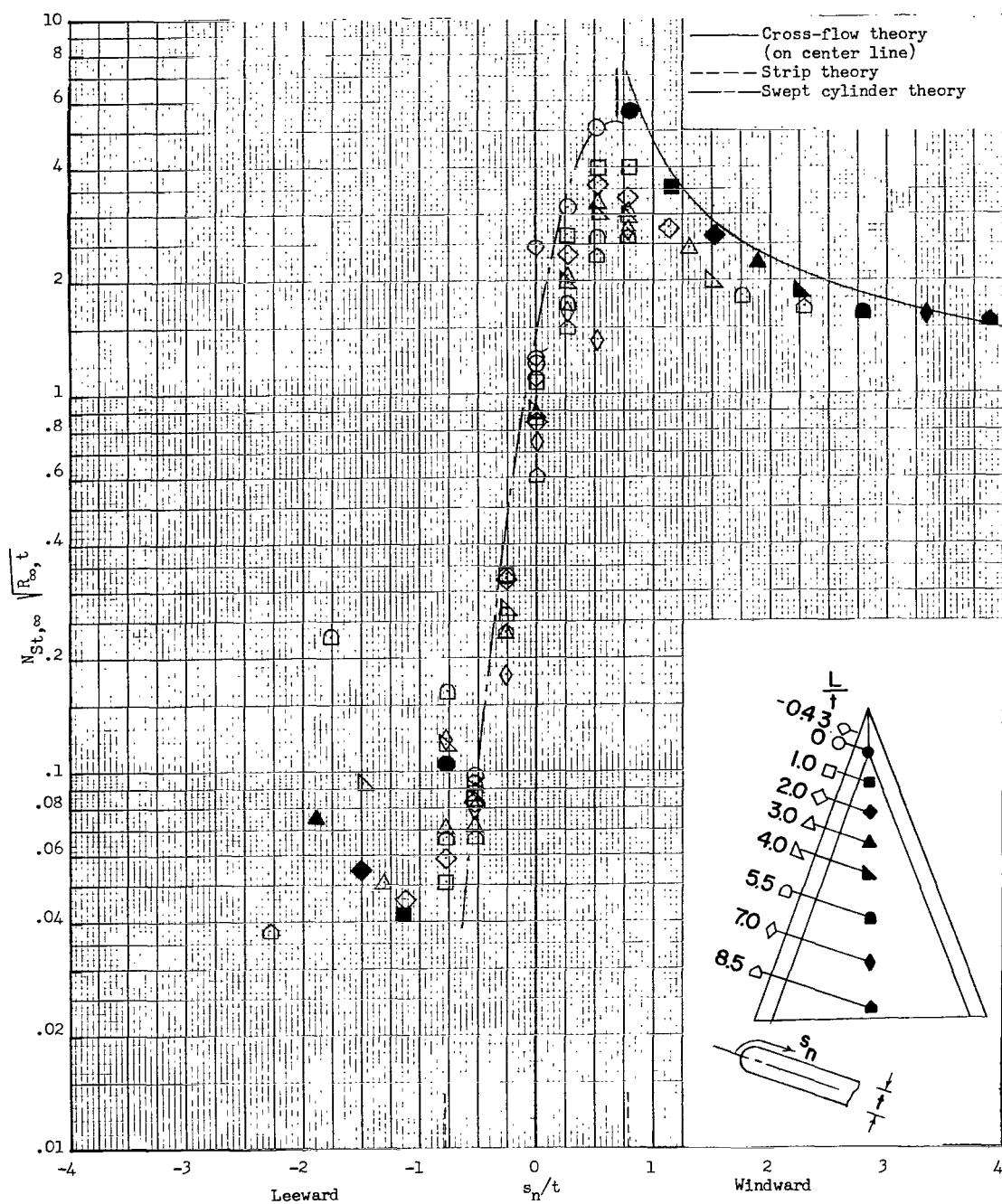
Figure 8.- Continued.

(h) $\alpha = 60°$.

Figure 8.- Continued.
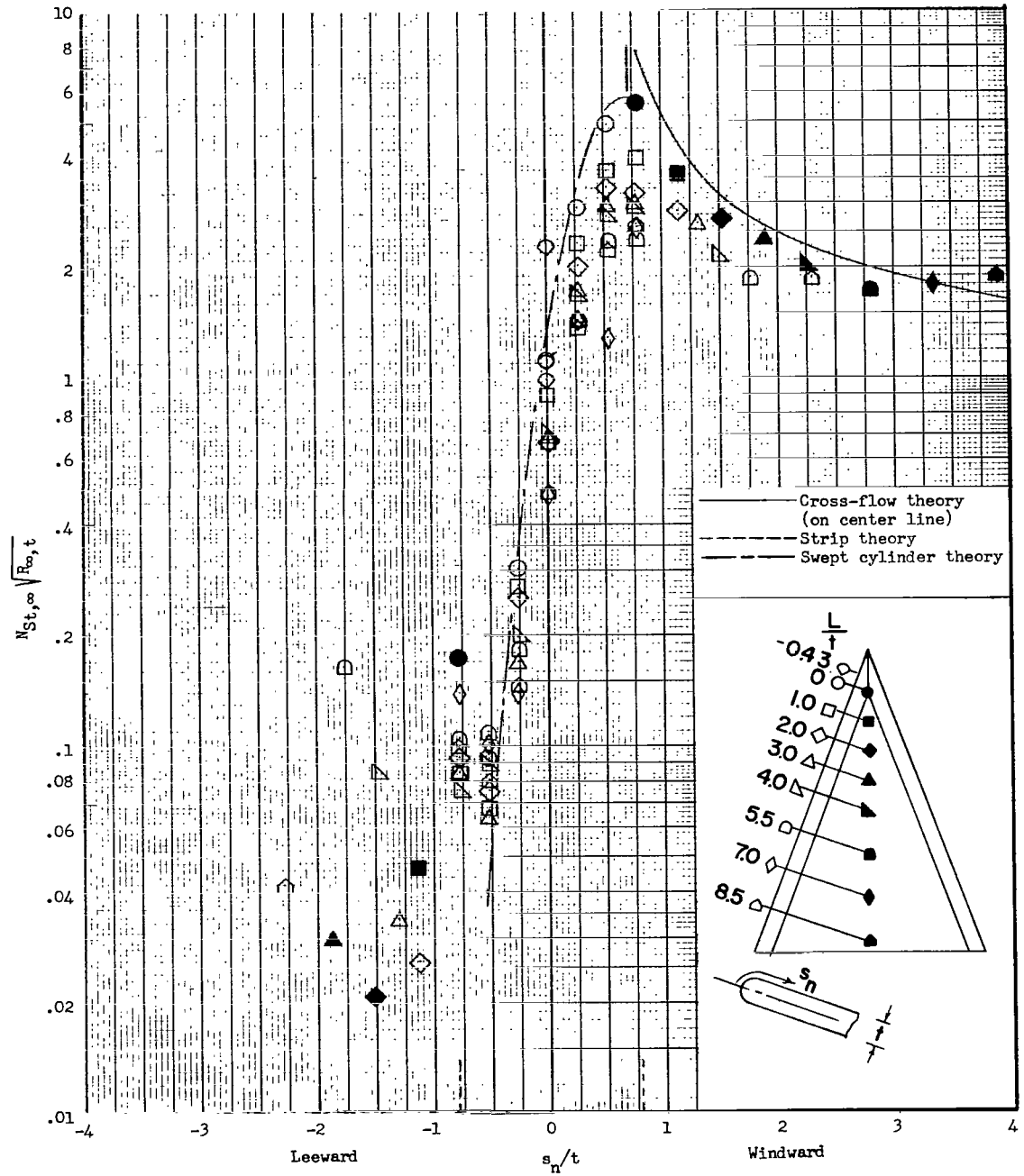
(i) α = 70°.

Figure 8.- Continued.
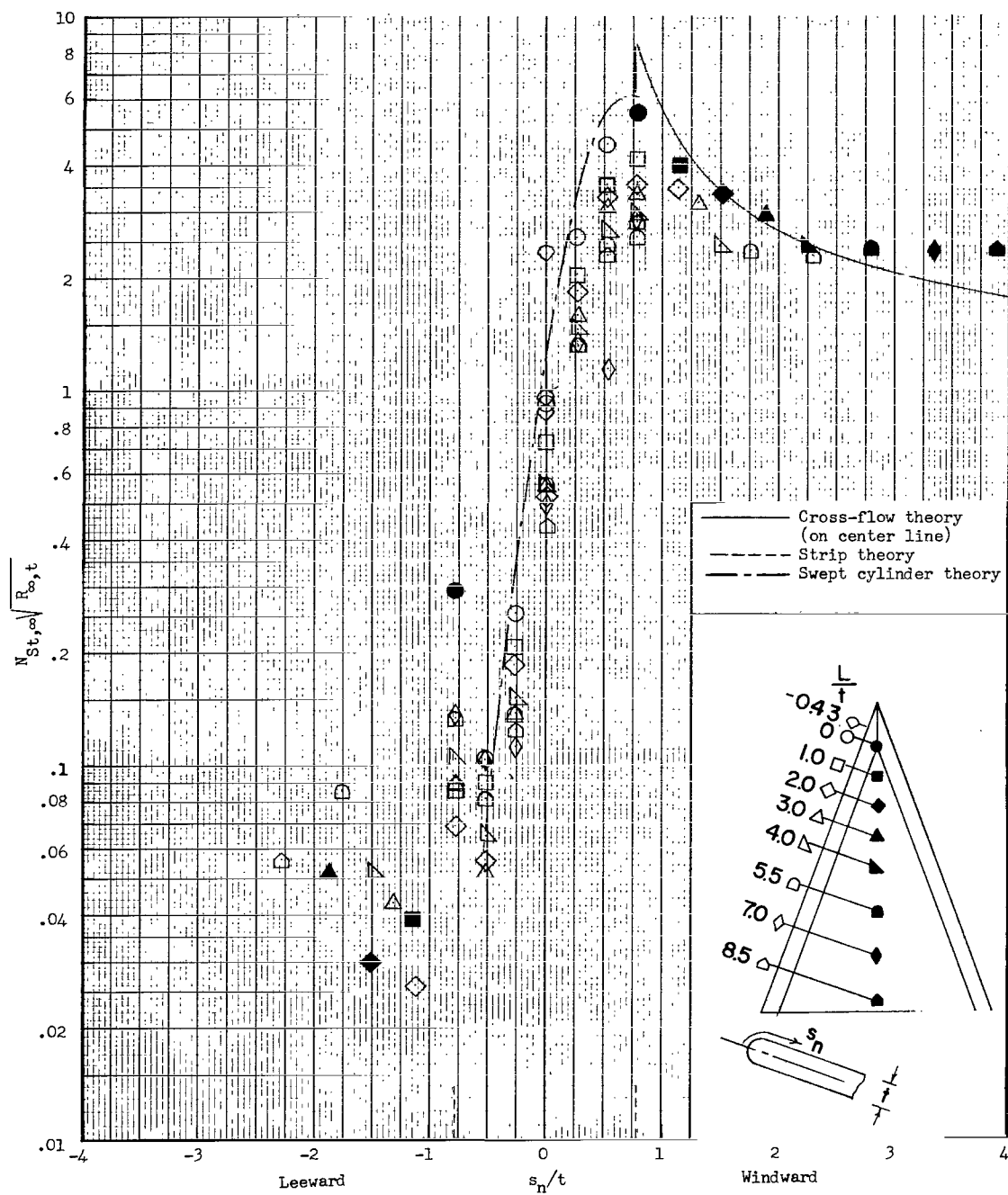
(j) $\alpha = 80^{\circ}$.

Figure 8.-.Continued.
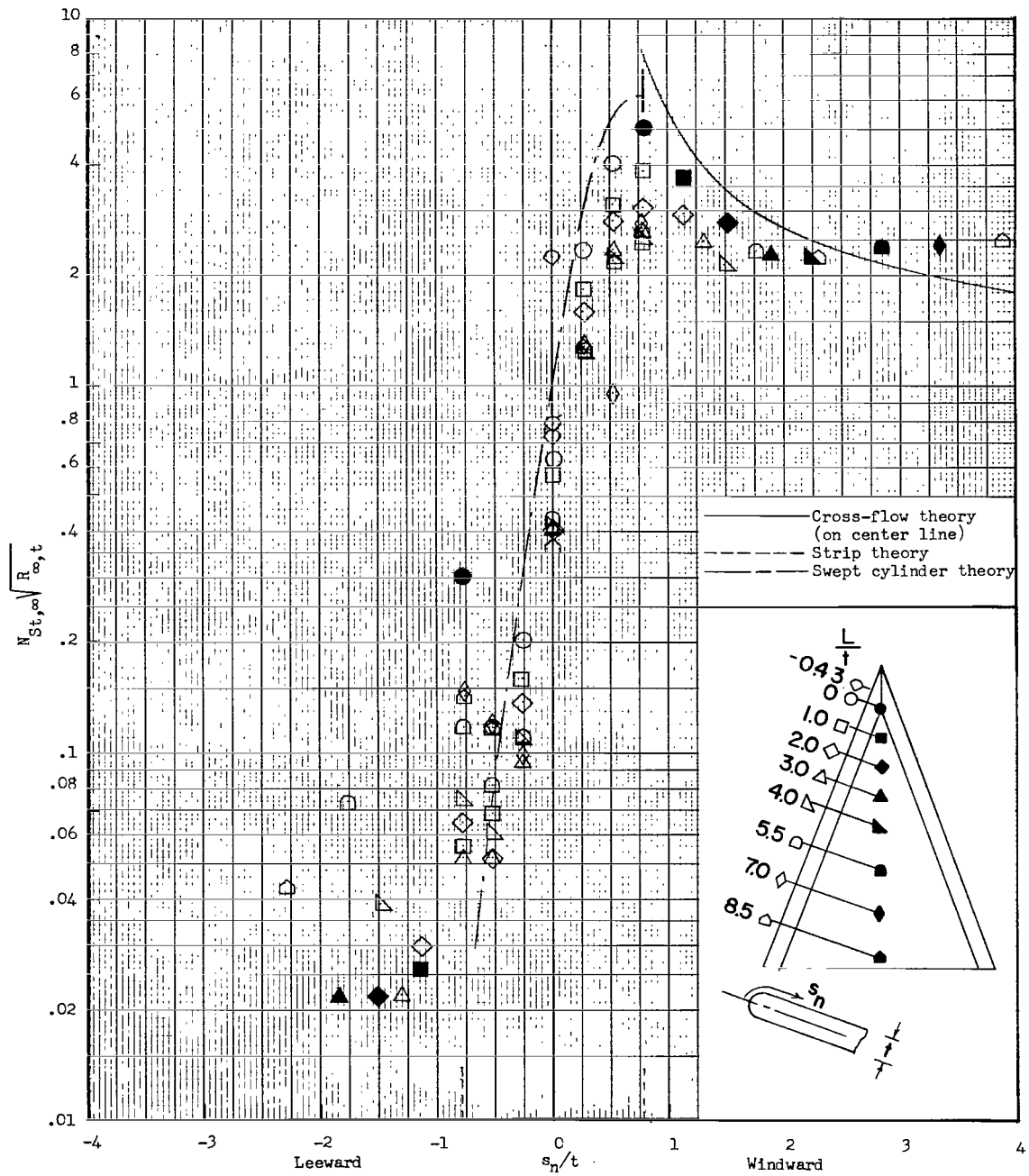
(k) $\alpha = 90^{\circ}$.

Figure 8.- Concluded.
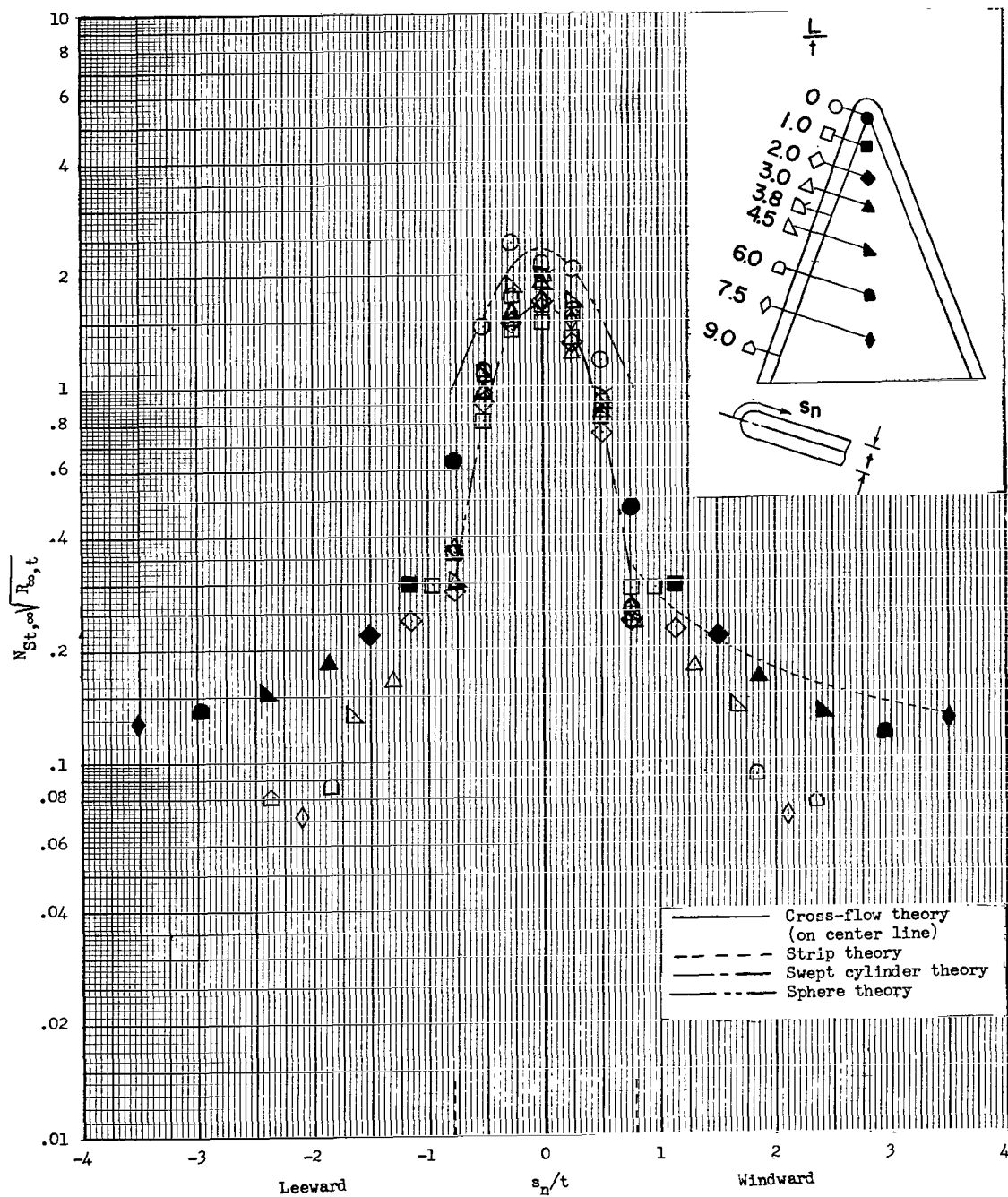
(a) $\alpha = 0^\circ$.

Figure 9.- Stanton number distribution normal to the leading edge on blunt-nose delta wing at various stations along the leading edge. Dashed vertical lines indicate juncture of leading edge and slab regions.
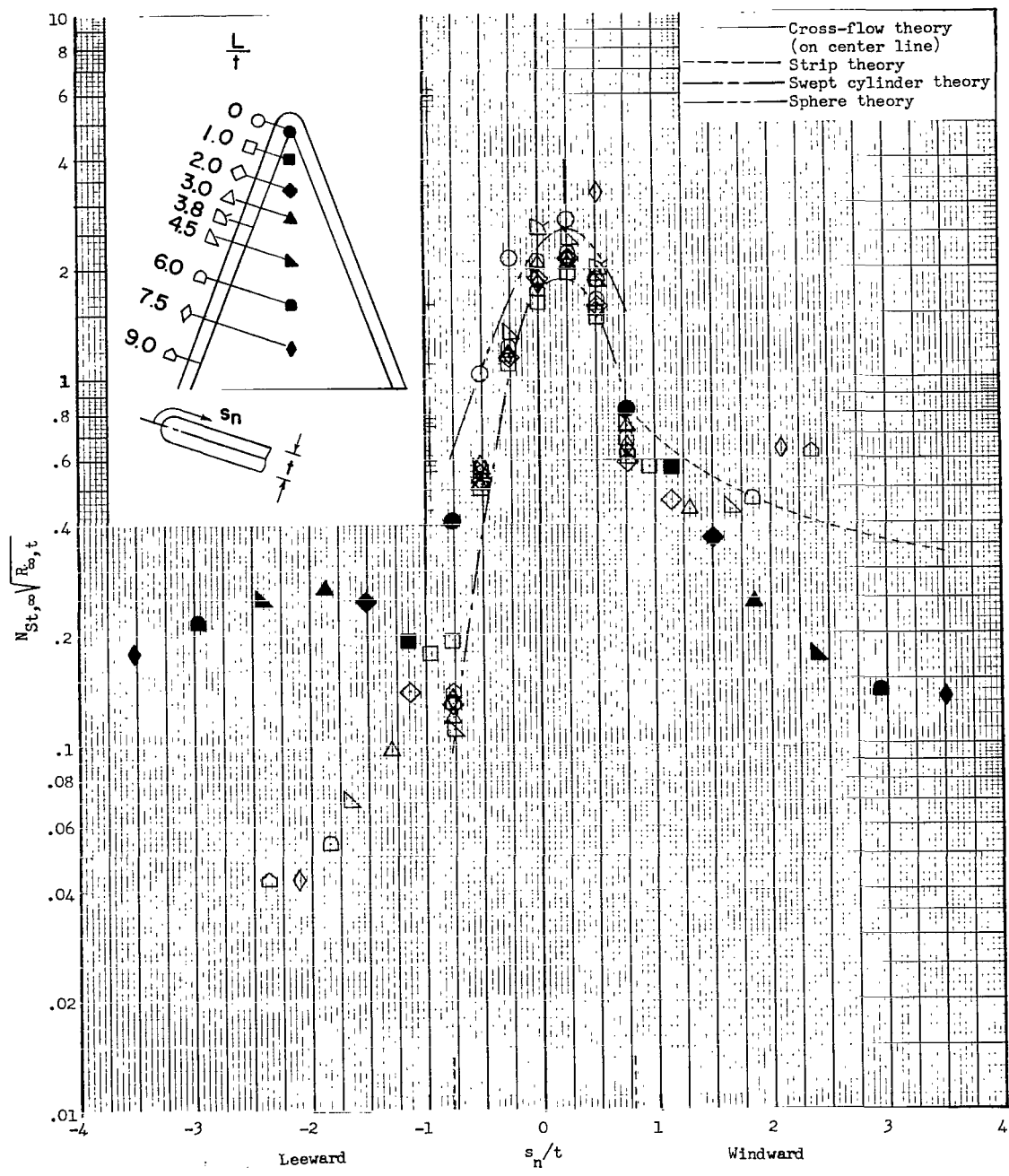
(b) $\alpha \approx 10°$.

Figure 9.- Continued.
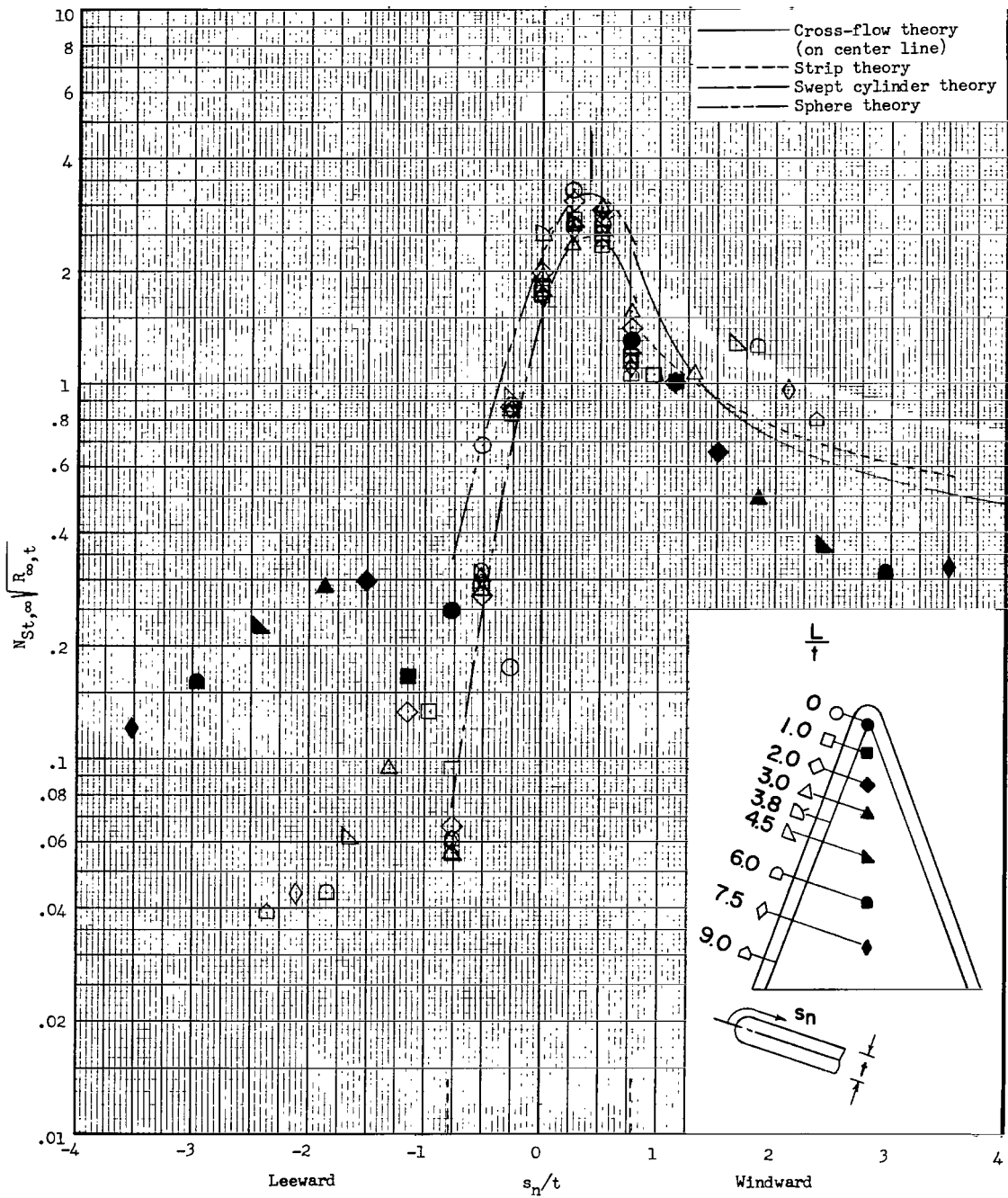
(c) $\alpha = 20°$.

Figure 9.- Continued.
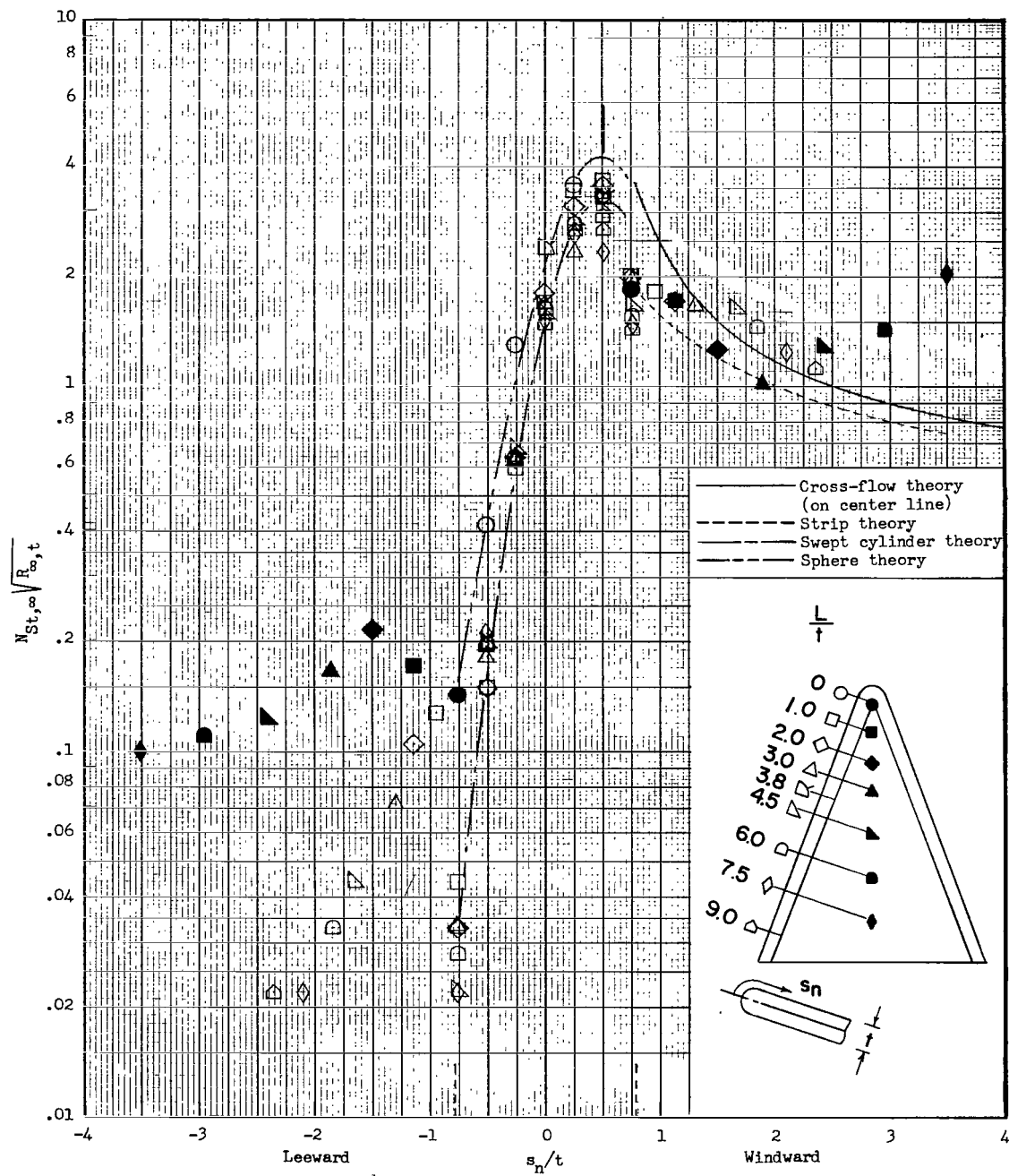
(d) α = 30°; model 2.

Figure 9.- Continued.
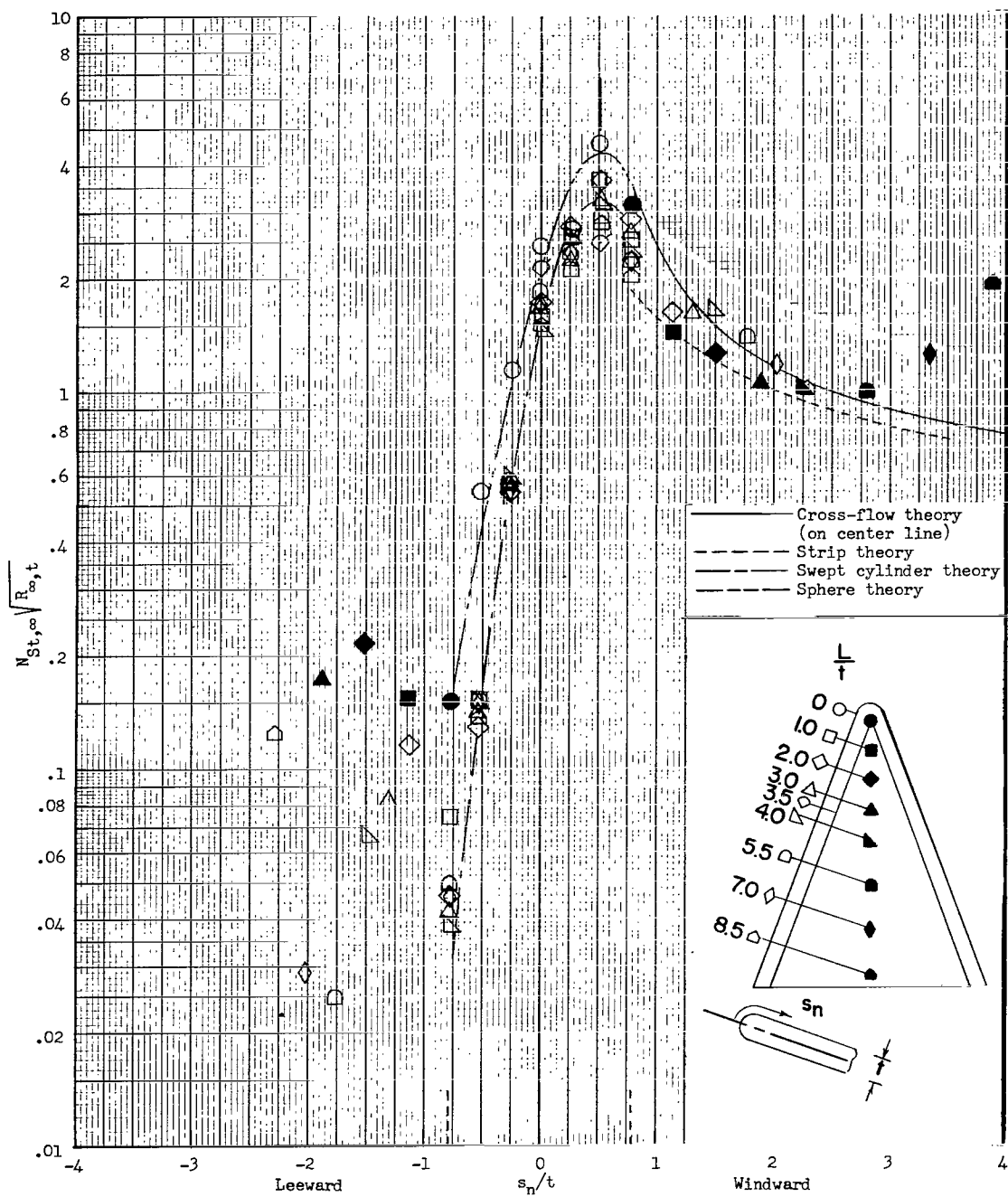
(e) $\alpha = 30^\circ$; model 4.

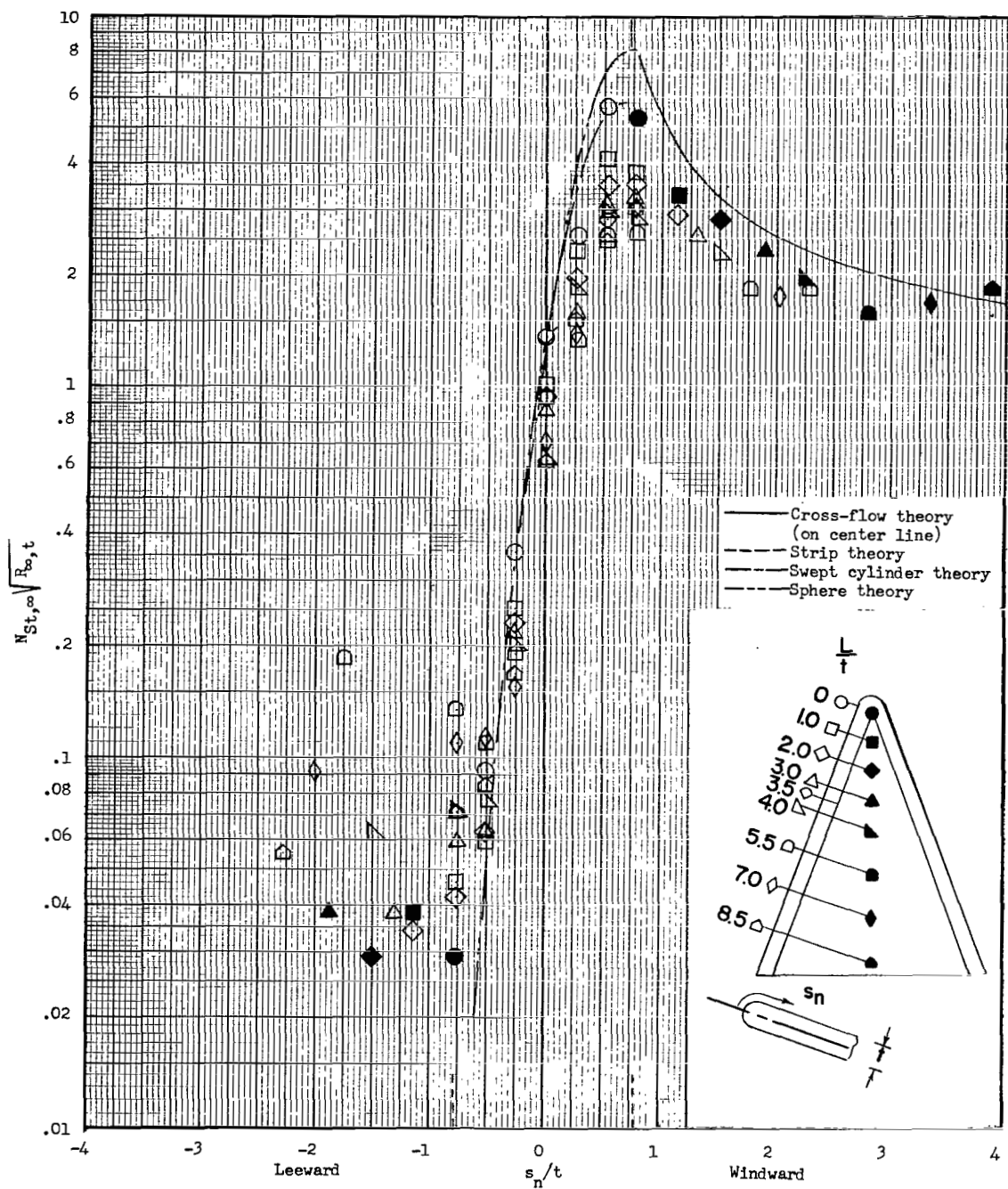Figure 9.- Continued.

(f) $\alpha = 40°$.

Figure 9.- Continued.
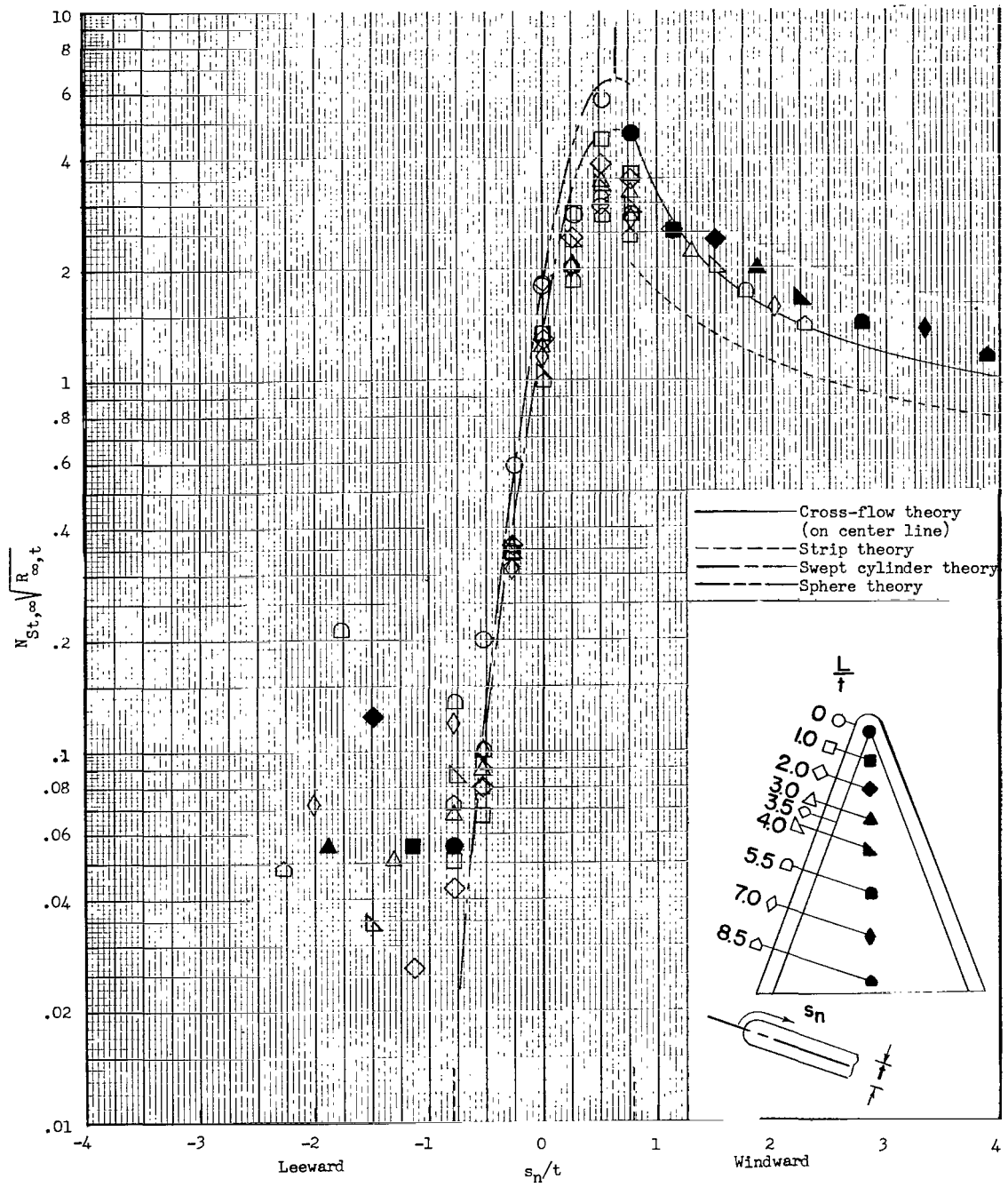
(g) α = 50°.

Figure 9.- Continued.
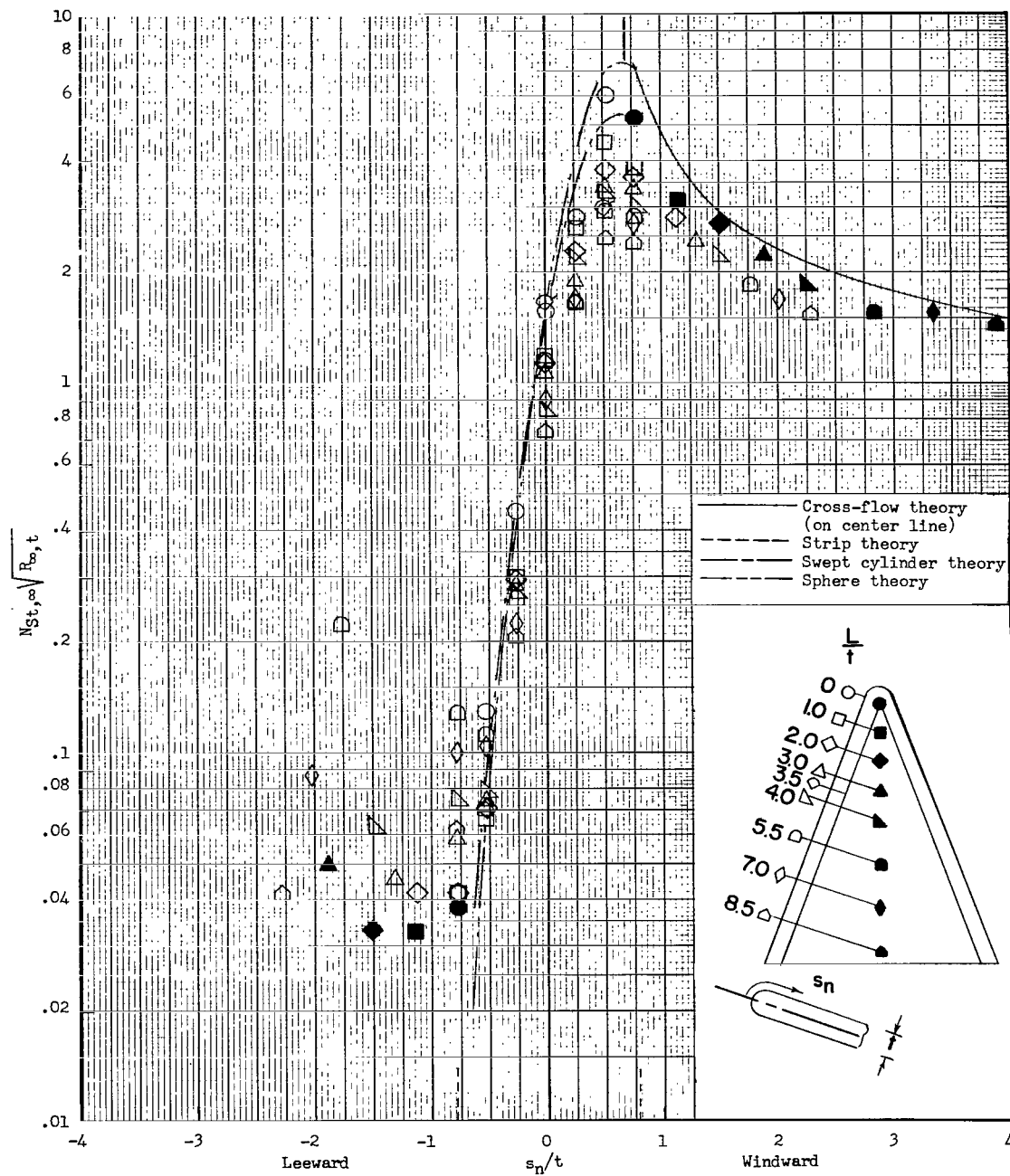
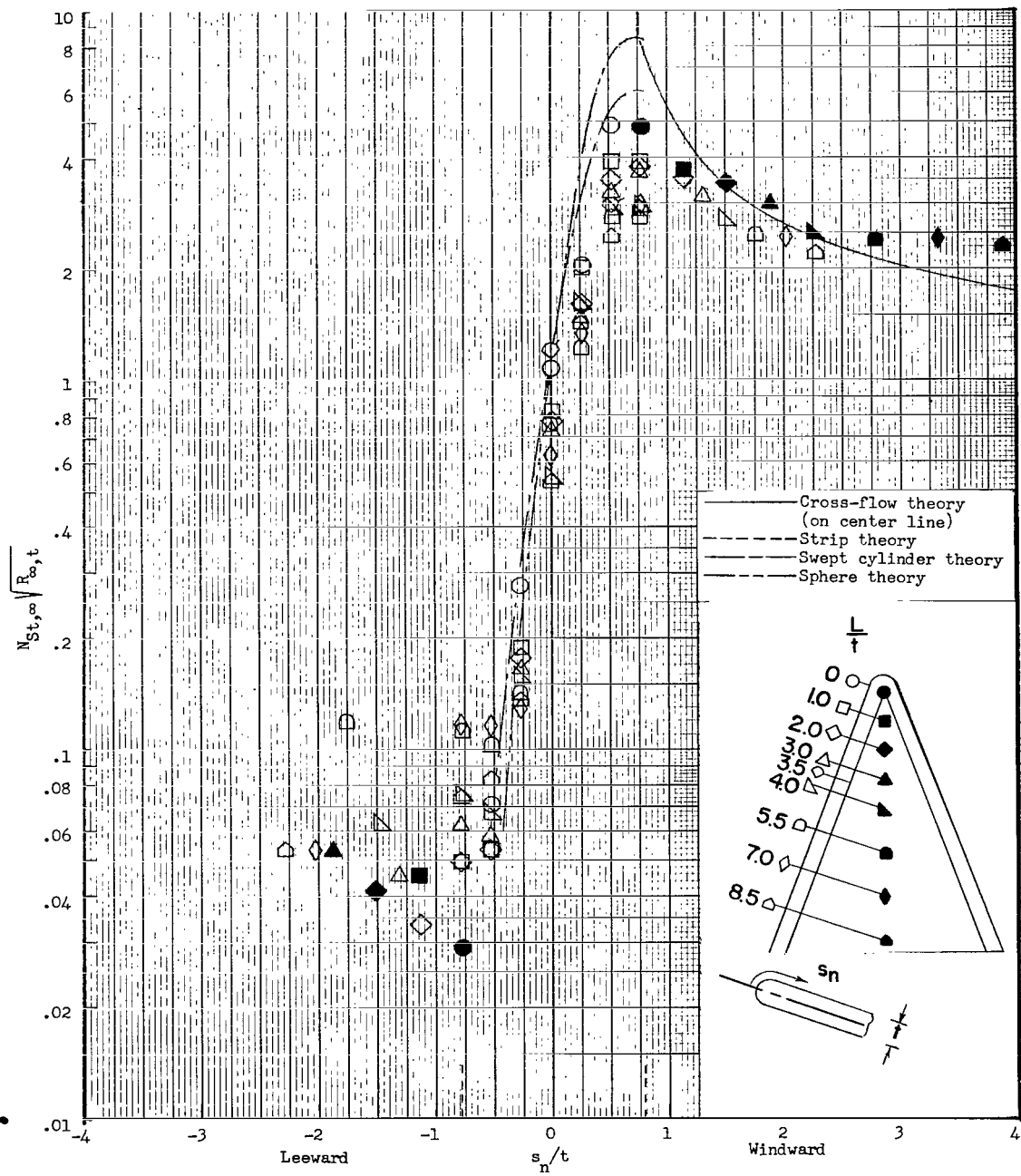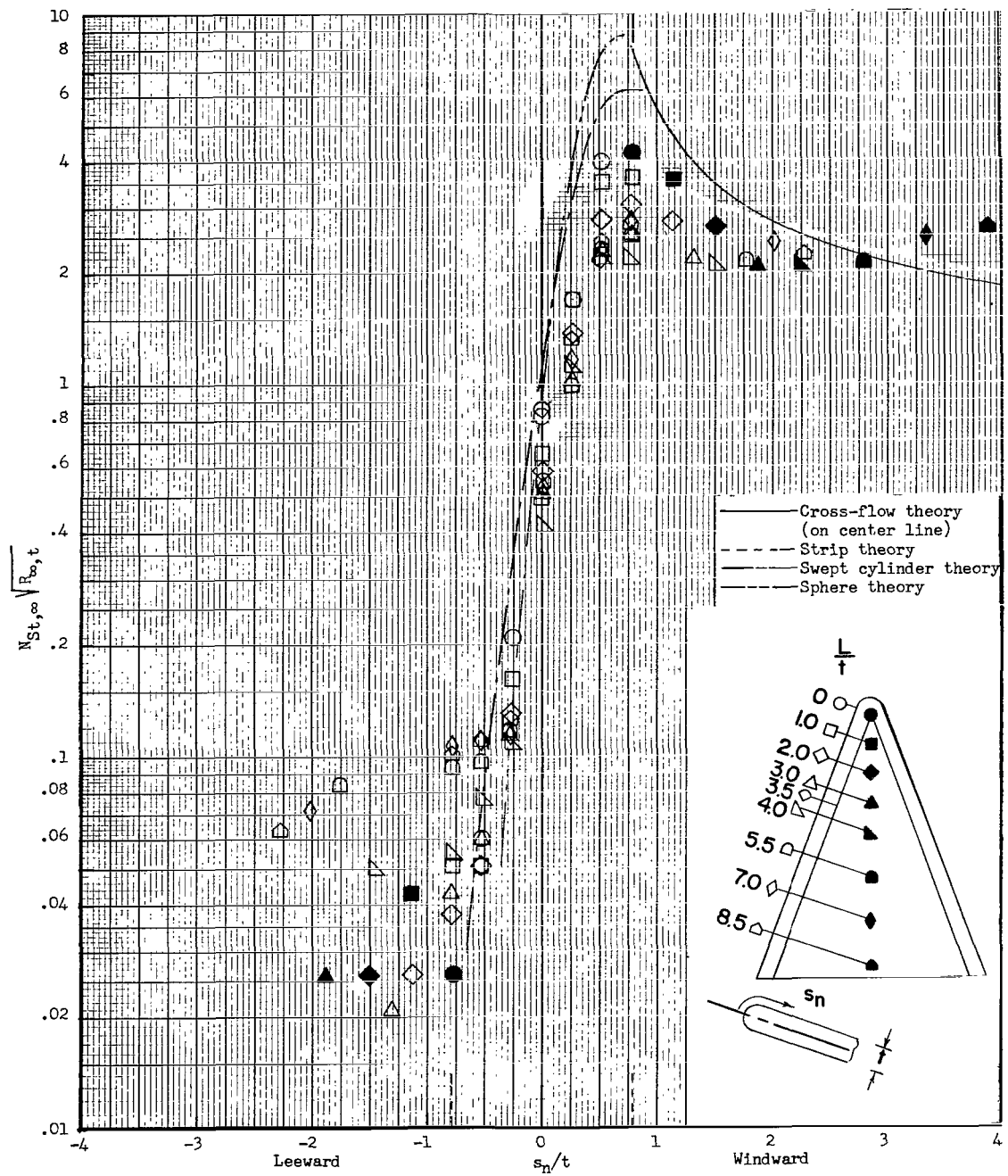(h) $\alpha = 60°$.
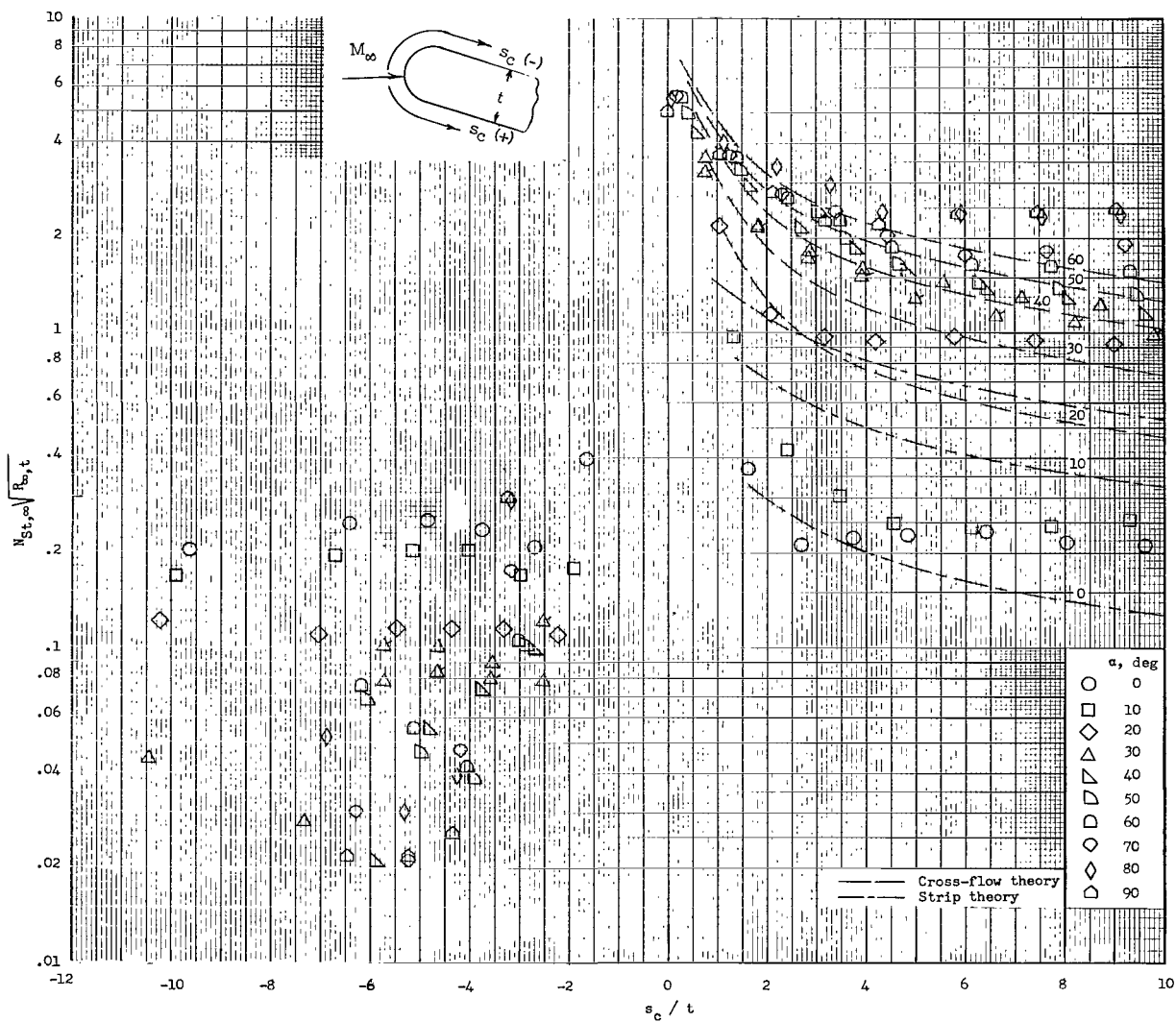
Figure 9.- Continued.

(1) α = 70°.

Figure 9.- Continued.

(j) $\alpha = 80°$.

Figure 9.- Continued.
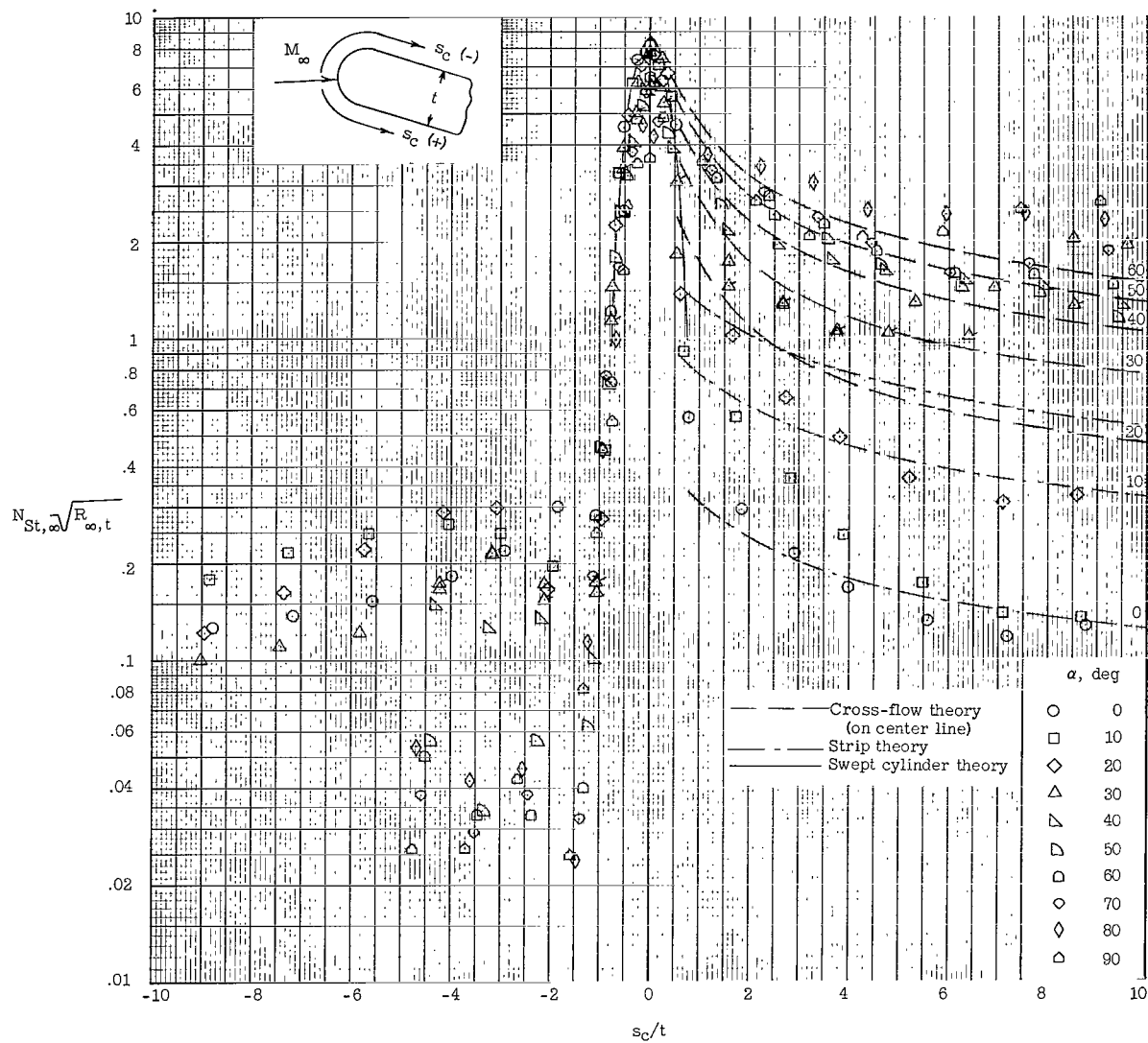
(k) $\alpha = 90°$.

Figure 9.- Concluded.

(a) Sharp-nose models.

Figure 10.- Center-line distribution of heat-transfer coefficient on slab delta wings.

(b) Blunt-nose models.

Figure 10.- Concluded.

"The aeronautical and space activities of the United States shall be conducted so as to contribute . . . to the expansion of human knowledge of phenomena in the atmosphere and space. The Administration shall provide for the widest practicable and appropriate dissemination of information concerning its activities and the results thereof."

—NATIONAL AERONAUTICS AND SPACE ACT OF 1958

NASA SCIENTIFIC AND TECHNICAL PUBLICATIONS

TECHNICAL REPORTS: Scientific and technical information considered important, complete, and a lasting contribution to existing knowledge.

TECHNICAL NOTES: Information less broad in scope but nevertheless of importance as a contribution to existing knowledge.

TECHNICAL MEMORANDUMS: Information receiving limited distribution because of preliminary data, security classification, or other reasons.

CONTRACTOR REPORTS: Technical information generated in connection with a NASA contract or grant and released under NASA auspices.

TECHNICAL TRANSLATIONS: Information published in a foreign language considered to merit NASA distribution in English.

TECHNICAL REPRINTS: Information derived from NASA activities and initially published in the form of journal articles.

SPECIAL PUBLICATIONS: Information derived from or of value to NASA activities but not necessarily reporting the results of individual NASA-programmed scientific efforts. Publications include conference proceedings, monographs, data compilations, handbooks, sourcebooks, and special bibliographies.

Details on the availability of these publications may be obtained from:

SCIENTIFIC AND TECHNICAL INFORMATION DIVISION

NATIONAL AERONAUTICS AND SPACE ADMINISTRATION

Washington, D.C. 20546